# Production of lightning NO$_x$ and its vertical distribution calculated from 3-D cloud-scale chemical transport model simulations

Lesley Ott, UMBC/GEST, Greenbelt, MD

Kenneth Pickering, NASA Goddard Space Flight Center, Greenbelt, MD

Georgiy Stenchikov, Rutgers University, New Brunswick, NJ

Dale Allen, University of Maryland, College Park, MD

Alex DeCaria, Millersville University, Millersville, PA

Brian Ridley, National Center for Atmospheric Research, Boulder, CO

Ruei-Fong Lin, UMBC/GEST, Greenbelt, MD

Steve Lang, SSAI, Greenbelt, MD

Wei-Kuo Tao, NASA Goddard Space Flight Center, Greenbelt, MD

29  Abstract

30          A 3-D cloud scale chemical transport model that includes a parameterized source

31  of lightning $NO_x$ based on observed flash rates has been used to simulate six midlatitude

32  and subtropical thunderstorms observed during four field projects. Production per

33  intracloud ($P_{IC}$) and cloud-to-ground ($P_{CG}$) flash is estimated by assuming various values

34  of $P_{IC}$ and $P_{CG}$ for each storm and determining which production scenario yields $NO_x$

35  mixing ratios that compare most favorably with in-cloud aircraft observations. We obtain

36  a mean $P_{CG}$ value of 500 moles NO (7 kg N) per flash. The results of this analysis also

37  suggest that on average, $P_{IC}$ may be nearly equal to $P_{CG}$, which is contrary to the common

38  assumption that intracloud flashes are significantly less productive of NO than are cloud-

39  to-ground flashes. This study also presents vertical profiles of the mass of lightning $NO_x$

40  after convection based on 3-D cloud-scale model simulations. The results suggest that

41  following convection, a large percentage of lightning $NO_x$ remains in the middle and

42  upper troposphere where it originated, while only a small percentage is found near the

43  surface. The results of this work differ from profiles calculated from 2-D cloud-scale

44  model simulations with a simpler lightning parameterization that were peaked near the

45  surface and in the upper troposphere (referred to as a "C-shaped" profile). The new

46  model results (a backward C-shaped profile) suggest that chemical transport models that

47  assume a C-shaped vertical profile of lightning $NO_x$ mass may place too much mass near

48  the surface and too little in the middle troposphere.

49

49    1.    Introduction

50         The oxides of nitrogen, (NO + $NO_2$ = $NO_x$), are important $O_3$ precursors in the

51    troposphere.  Of the major sources of $NO_x$ in the troposphere, lightning remains the

52    source with the greatest uncertainty and is particularly important because it produces $NO_x$

53    in the middle and upper troposphere where $NO_x$ is longer lived and can be more efficient

54    at producing ozone than in the boundary layer. The representation of lightning $NO_x$

55    ($LNO_x$) in three-dimensional (3-D) regional and global chemical transport models

56    (CTMs) is critical to the models' representation of ozone and other species such as OH

57    [e.g. Stockwell et al., 1999, Labrador et al., 2004].  Labrador et al. [2005] found that both

58    the magnitude of the global $LNO_x$ source strength and its vertical distribution can

59    substantitally affect tropospheric trace gas concentrations in a global CTM.  IPCC [2007]

60    suggests a global $LNO_x$ source of 1.1-6.4 Tg N $yr^{-1}$ based on the work of Boersma et al.

61    [2005].  However, Schumann and Huntrieser et al. [2007] have comprehensively

62    summarized estimates of global $LNO_x$ production and found the best estimate to be 5±3

63    Tg N $yr^{-1}$.

64         In order to adequately represent the $LNO_x$ source in global or regional models, the

65    geographic distribution of flashes, average production of NO per flash, and vertical

66    distribution of $LNO_x$ following convection must be specified.  A variety of schemes have

67    been used to specify the horizontal distribution of flashes (e.g. using variables such as

68    cloud-top height, upward cloud mass flux, convective preciptation, and CAPE as

69    predictors).  Allen and Pickering [2002] have evaluated their use in global 3-D CTMs.

70    The production of NO per flash has also been examined using laboratory experiments,

71    theoretical assumptions regarding the physics of lightning flashes, and observations

72    obtained during field projects.  Despite these efforts, a great deal of uncertainty remains

73      regarding NO production on a per flash basis, as well as the relative production by

74      intracloud (IC) and cloud-to-ground (CG) flashes. On the basis of previous studies,

75      which suggested that IC flashes were less energetic than CG flashes (e.g. Holmes et al..

76      1971), many studies of lightning $NO_x$ production have assumed that $P_{IC}$ is less than $P_{CG}$.

77      Price et al. [1997] assumed that a CG flash produces approximately 1100 moles of NO

78      and that an IC flash was one tenth as productive of NO as a CG flash in estimating global

79      lightning $NO_x$ production.

80          However, a number of more recent studies have suggested that $P_{IC}$ may be nearly

81      as great as $P_{CG}$. Gallardo and Cooray [1996] suggested that IC flashes may dissipate

82      nearly as much energy as CG flashes and therefore $P_{IC}$ may be on the order of $P_{CG}$.

83      Supporting the Gallardo and Cooray [1996] hypothesis, a two-dimensional (2-D) cloud-

84      scale modeling study by DeCaria et al. [2000] suggested that the $P_{IC}/P_{CG}$ ratio is likely

85      between 0.5 and 1.0 and a 3-D modeling analysis by DeCaria et al. [2005] narrowed this

86      range to between 0.75 and 1.0. A study by Fehr et al. [2004] used a 3-D cloud-scale

87      model simulation of a storm observed over Germany, and by comparing with lightning

88      and aircraft observations, concluded that on average, an IC flash produced 40% more NO

89      than a CG flash. Zhang et al. [2003] argued that IC flashes may dissipate 50-100% as

90      much energy as CG flashes because they have a large number of return strokes which

91      where neglected in the Price et al. [1997) calculations. Rahman et al. [2007] found that

92      results from experiments with rocket-triggered lightning suggested that $NO_x$ production

93      was associated with relatively long duration continuing currents, which may be greater in

94      IC flashes than in CG flashes, leading to the implication that IC flashes may produce as

95      much or possibly more $NO_x$ per flash than CG flashes. Recent estimates of energy

96      dissipated by IC and CG flashes using electrical potential and charge density

97    measurements by Maggio et al. [2008] also suggest IC flashes may dissipate as much or

98    more energy than CG flashes.

99           Pickering et al. [1998] presented vertical profiles of lightning $NO_x$ for use in 3-D

100    CTMs based on the results of 2-D cloud-resolving model simulations of seven convective

101    events. These simulations assumed the production scheme of Price et al. [1997]. $NO_x$

102    produced by CG flashes was distributed in the simulated storms from the surface to the -

103    15°C isotherm while $NO_x$ produced by IC flashes was distributed from the -15°C

104    isotherm to the cloud top. Average profiles of $LNO_x$ mass computed for the midlatitude

105    continental, tropical continental, and tropical marine regimes showed peaks in mass near

106    the surface and in the upper troposphere, leading many CTMs to adopt a C-shaped

107    vertical distribution of $LNO_x$ mass.

108           This paper has two primary objectives: (1) to summarize the results of 3-D cloud-

109    resolved storm simulations yielding estimates of NO production per flash and (2) to

110    update the vertical $LNO_x$ profile information of Pickering et al. [1998]. Six storms from

111    field projects conducted in Germany, Colorado, south Florida, and Kansas/Oklahoma

112    have been simulated using a 3-D cloud-scale chemical transport model (CSCTM) that

113    includes a parameterized source of $LNO_x$. $LNO_x$ production per flash is estimated

114    individually for five of the six storms. In this study we present vertical distributions of

115    $LNO_x$ calculated from each of these 3-D simulations as well as average vertical profiles

116    for the midlatitude continental and subtropical events, which can be applied in regional

117    and global CTMs. Section 2 describes the methodology used in these studies, while

118    section 3 presents results from the individual storm simulations. Section 4 discusses the

119    results of the storm case studies and their application to global models and remote

120    sensing. Section 5 presents conclusions that may be drawn from this work.

121   2.      Methodology

122          Storms from the Cirrus Regional Study of Tropical Anvils and Cirrus Layers –

123   Florida Area Cirrus Experiment (CRYSTAL-FACE; Ridley et al., 2004; Lopez et al.,

124   2006), European Lightning Nitrogen Oxides Project (EULINOX; Huntrieser et al, 2002),

125   Stratosphere Troposphere Experiment: Radiation, Aerosols and Ozone (STERAO; Dye et

126   al., 2000), and Preliminary Regional Experiment for STORM (PRE-STORM; Rutledge

127   and MacGorman, 1988) field projects were simulated.  With the exception of the PRE-

128   STORM event, all of these storms featured measurements of chemical and

129   meteorological properties by research aircraft at anvil levels.  The time, location, and

130   peak current of CG lightning occurrences in all storms were recorded by ground-based

131   systems, and during STERAO and EULINOX, total lightning activity (IC + CG) was

132   mapped by a VHF interferometer.  In addition, all experiments included extensive

133   satellite and radar observations of storm development and evolution.

134          The dynamical evolution of each storm was simulated using a cloud-resolving

135   model and the temperature, wind, and hydrometeor fields were then used to drive the

136   offline CSCTM.  For each storm, various $LNO_x$ production per flash scenarios were

137   simulated and model results were compared with in-cloud aircraft observations of $NO_x$

138   through use of mean profiles, column $NO_x$ mass, and probability distribution functions of

139   simulated and observed $NO_x$ to determine the most appropriate scenario.  At the end of

140   the CSCTM simulation, the mass of N fixed by lightning was calculated at each model

141   level, and the percentage of the total mass of $LNO_x$ was calculated for 1-km layers.

142          A detailed description of the CSCTM is found in DeCaria et al. [2005]. In this

143   version of the model, $LNO_x$ production is computed using observed IC and CG flash

144   rates and a specified scenario of $P_{IC}$ and $P_{CG}$ to calculate the mass of NO injected into the

6

145 cloud per time step. Both laboratory experiments (Wang et al., 1998) and theoretical

146 considerations (Price et al., 1997) have pointed to a strong dependence of $LNO_x$

147 production on stroke peak current. Therefore, we have made initial estimates of $P_{CG}$

148 using these relationships because peak current data for return strokes are available from

149 ground-based network observations of CG flashes. However, this assumption contributes

150 to uncertainty in the results because recent work with rocket-triggered lightning (Rahman

151 et al., 2007) has suggested that return strokes are not the primary NO-producing phase of

152 a lightning flash. Field experimental results from TROCCINOX (Tropical Convection,

153 Cirrus and Nitrogen Oxides Experiment) in Brazil (Huntrieser et al., 2008) have

154 suggested a more minor dependence on stroke peak current.

155       The NO produced by CG flashes is distributed unimodally in the vertical, while

156 the NO produced by IC flashes is distributed bimodally based on the vertical distributions

157 of very high frequency (VHF) sources of IC and CG flashes presented in MacGorman

158 and Rust [1998]. The two modes correspond to the two main charge centers in a typical

159 thunderstorm cloud. The vertical distributions of IC and CG lightning channels used in

160 the model are shown in Figure 2 of DeCaria et al. [2005]. The modes of the IC

161 distribution are nominally set at the heights of the -15°C and -45°C isotherms. However,

162 the vertical distribution of IC channels is modified as necessary in some storms by

163 changing the upper mode isotherm to account for a higher or lower cloud top and to

164 match the upper tropospheric peak in aircraft observations of $NO_x$. At each model level,

165 the lightning NO is distributed uniformly to all grid cells within the 20 dBZ contour

166 computed from simulated hydrometeor fields. A passive version of the CSCTM includes

167 only the transport of tracer species and production of lightning $NO_x$. In this version,

168 three types of $NO_x$ (pre-existing $NO_x$, CG $LNO_x$, and IC $LNO_x$) are transported without

169    any chemical reactions and the results are used to estimate average $NO_x$ produced by IC

170    and CG flashes.  Various production scenarios are specified and the model results

171    compared with in-cloud aircraft observations to determine a first estimate of the most

172    appropriate $LNO_x$ production scenario for the storm in question.

173          A version of the model that includes $O_3$ photochemistry is used to separate $NO_x$

174    into NO and $NO_2$ and obtain a final and best estimate of NO production by IC and CG

175    flashes.  The chemical mechanism for the STERAO storms is described in DeCaria et al.

176    [2005].  In the CRYSTAL-FACE and EULINOX simulations, the chemical scheme is

177    identical to that described in DeCaria et al. [2005] with the exception that in these cases,

178    isoprene and propene chemistry was included.  Initial profiles of ozone were constructed

179    using out-of-cloud aircraft observations, and when necessary to fill gaps, climatological

180    ozone profiles appropriate for the latitude of the storm in question.  The CSCTM includes

181    a simple scheme to represent the influence of clouds on photolysis rates based on the

182    work of Madronich [1987] and fully described in DeCaria et al. [2005].  Clear sky

183    photolysis rates are calculated following Stamnes et al. [1988] using observed column

184    ozone amounts measured by the Total Ozone Mapping Spectrometer (TOMS) or, in the

185    case of the STERAO storms, ozonesondes launched from Boulder, Colorado.

186    Perturbations to clear sky photolysis rates are determined by cloud thickness with very

187    thick clouds (deeper than 5 km) resulting in photolysis rates multiplied by a factor of 2

188    above the cloud and 0.1 below the cloud base with a linearly interpolated degree of

189    enhancement at intermediate altitudes.

190    3.    Results

191    3.1    Subtropical Events

8

192     The CRYSTAL-FACE experiment was conducted over South Florida in July,

193     2002 and two storms investigated during the campaign were simulated. The July 29

194     CRYSTAL-FACE storm was simulated using the NASA Goddard version of the non-

195     hydrostatic PSU/NCAR (MM5) mesoscale model (Tao et al., 2003b) with a horizontal

196     resolution of 2 km and vertical resolution of 0.5 km. At 1700 UTC (1300 LT) on July 29,

197     2002, a powerful thunderstorm developed along the west coast of Florida near Fort

198     Myers. While the storm intensified and moved north along the coast, the area in and

199     above the anvil was sampled by the NASA WB-57 research aircraft from 1845 to 2011

200     UTC at altitudes ranging from 12.5 to 13.8 km. The coastal convection later merged with

201     convection originating near Lake Okeechobee. Figure 1 shows the time series of CG

202     flashes recorded by the National Lightning Detection Network (NLDN) from 1700 to

203     2300 UTC. The July 29 storm was an exceptionally strong lightning producer with 4168

204     CG flashes recorded during this period. Maximum CG flash rates exceed 30 flashes per

205     minute. These lightning flash rates and their relationship to NO observations from the

206     WB-57 aircraft have been discussed by Ridley et al. [2004].

207     Simulated convection along the coast began earlier than observed by

208     approximately three hours, but a number of storm features were successfully reproduced,

209     including cloud top height and the direction of storm movement. The transport of CO

210     (initial boundary layer maximum) and $O_3$ (initial stratospheric maximum) were calculated

211     by the CSCTM and compared with in-cloud observations using probability distribution

212     functions (pdfs). The model overestimated the frequency of values in the upper end of

213     the frequency distributions for both CO and $O_3$ at anvil levels, suggesting that both

214     upward and downward transport in the model may be too strong. However, the intense

215     lightning activity in the thunderstorm and extremely elevated $NO_x$ mixing ratios (up to 10

216    ppbv) observed in the anvil indicate that the lightning $NO_x$ source in this storm was

217    extremely strong. As a result, errors in transport are unlikely to significantly affect the

218    estimate of $LNO_x$ production per flash in this case.

219    Because the NLDN only recorded the occurrence of CG flashes during

220    CRYSTAL-FACE, IC flashrates were estimated for the July 29 storm. NLDN flashes

221    with positive peak current less than 10 kA are thought to be IC flashes [Cummins et al.,

222    1998]. These flashes were removed from the NLDN observations to estimate CG flash

223    rates. The percentage of recorded flashes with positive peak current less than 10 kA was

224    calculated during both the July 29 storm and the month of July as a whole. The

225    percentage of such flashes in the July 29 storm was larger by a factor of 2.5 than the

226    percentage for the month of July which may indicate an enhancement of the IC/CG ratio

227    in the July 29 storm over the climatological value. To account for this enhancement, the

228    south Florida climatological value for the IC/CG ratio of 2 from Boccippio et al. [2001]

229    was multiplied by 2.5 to estimate an IC/CG ratio of 5. The upper mode of the vertical

230    distribution of IC flash channel segments was set to -45°C.

231    $P_{CG}$ was estimated to be approximately 590 moles NO based on observed mean

232    peak current (19 kA) and a relationship between peak current and energy dissipated from

233    Price et al. [1997]. Various values of the $P_{IC}/P_{CG}$ ratio were simulated and the results

234    compared with aircraft $NO_x$ observations (observed NO + estimated $NO_2$). $NO_2$ was

235    estimated using NO and $O_3$ observations and the photostationary state assumption

236    because no direct measurements of $NO_2$ were available. Following the work of

237    Madronich (1987), who demonstrated that actinic flux and photodissocation could

238    increase within clouds, $NO_2$ mixing ratios were calculated assuming both clear sky

239    photolysis rates and rates enhanced by a factor of 2. The observed column mass of N in

240     $NO_x$ was calculated for the 1 km thick layer extending from 12.25 to 13.25 km by

241     computing layer mean in-cloud $NO_x$ mixing ratios. Assuming that photolysis rates were

242     enhanced in the cloud yielded a column mass of $6.6 \times 10^{-4}$ g N m$^{-2}$ while assuming that

243     photolysis rates were unaltered by the cloud yielded a column mass of $7.0 \times 10^{-4}$ g N m$^{-2}$.

244     Table 1 shows the sensitivity of CSCTM-calculated column mass to the assumed $P_{IC}/P_{CG}$

245     ratio. Assuming that an IC flash is on average 60% as productive of NO as a CG flash

246     yields the most favorable comparison with column mass of nitrogen estimated from

247     aircraft observations when an IC/CG ratio of 5 is assumed.

248        Figure 2 shows the pdfs of observed and simulated in-cloud $NO_x$ assuming that

249     $P_{IC}$ equals 50 and 60% of $P_{CG}$ and an IC/CG ratio of 5. When compared with observed

250     pdfs at both 12.5 and 13 km, the production scenario that assumes a $P_{IC}/P_{CG}$ ratio of 0.5

251     compares more favorably than assuming a $P_{IC}/P_{CG}$ ratio of 0.6. The pdfs show that the

252     underestimation of the simulated column mass assuming a $P_{IC}/P_{CG}$ ratio of 0.5 results

253     from the inclusion of gridcells with background $NO_x$ concentrations as well as the

254     underestimation of the distribution at 13 km between 2 and 6 ppbv. Based on the

255     comparison of simulated and observed pdfs and computed column mass, it is estimated

256     that in the July 29 CRYSTAL-FACE storm an IC flash on average produced 50-60% as

257     much NO as a CG flash while an average CG flash produced 590 moles NO. The

258     assumption that an IC flash is one tenth as productive of NO as a CG flash significantly

259     underestimated $NO_x$ when compared to column mass estimates calculated from in-cloud

260     aircraft observations. When chemical reactions were simulated in addition to lightning

261     $NO_x$ production and convective transport, a loss of $NO_x$ occurred due to conversion to

262     reservoir species. The simulated column mass of N in $NO_x$ decreased by approximately

263     5% from the values shown in Table 1. The $P_{IC}/P_{CG}$ ratio of 0.6 was selected for the

264  subsequent calculations because it continued to provide the best comparison with the

265  column mass estimates derived from aircraft. It should be noted that the production

266  scenario discussed above was deduced assuming that the IC/CG ratio in this particular

267  storm was greater than the climatological IC/CG ratio for south Florida by a factor of 2.5.

268  Because many more weak positive flashes (which are believed to be IC flashes) were

269  recorded in this storm than was typical for the South Florida area during the month of

270  July, it is likely that the IC/CG ratio was elevated above the climatological value. If

271  instead the climatological IC to CG ratio of 2 is assumed, an IC flash must produce 50%

272  more NO than a CG flash to match aircraft observations.

273          It should be noted that the assumptions of IC/CG ratio, $P_{CG}$ value, and $P_{IC}/P_{CG}$

274  ratio contribute to uncertainty in the production scenario estimate. Figure 3 shows all the

275  possible production scenarios that yield $NO_x$ mixing ratios which would match observed

276  column mass when IC/CG ratios of 2 or 5 are assumed. The symbols on the curves show

277  our best estimates ($P_{CG}$ = 590 moles/flash with $P_{IC}/P_{CG}$ at 0.6 and 1.5) based on the

278  observed mean peak current. Most literature estimates of $P_{CG}$ range from 200 to 1100

279  moles NO per flash. For this range of $P_{CG}$ values, the $P_{IC}/P_{CG}$ ratio could range from 0.3

280  to 4 in the July 29 CRYSTAL-FACE storm. If $P_{IC}$ is assumed to equal $P_{CG}$, then $P_{CG}$

281  must be between 350 and 850 moles NO per flash depending on the number of IC flashes

282  which are assumed to have occurred. This analysis puts bounds on the uncertainty

283  associated with assuming a single production scenario. If the IC/CG ratio was known to

284  be 5 for this storm, the uncertainty would be reduced. $P_{IC}/P_{CG}$ would be in the 0.3 to 1.8

285  range (assuming $P_{CG}$ is between 200 and 1100 moles NO per flash). The assumption that

286  IC and CG lighting are equally productive of NO on a per flash basis would yield a

287  production of 350 moles NO per flash. This analysis demonstrates the need for

288      observations of IC flashes in future experiments and more definitive information on the

289      relationship between peak current or other electrophysical variables and $LNO_x$

290      production.

291          A vertical cross section of simulated $NO_x$ through the core of the coastal storm at

292      the end of the 240 minute simulation is shown in Figure 4 (assuming $P_{CG}$ = 590 moles

293      NO, $P_{IC}$ = 354 moles NO, and an IC/CG ratio of 5). Maximum $NO_x$ mixing ratios exceed

294      11 ppbv in the convective plume extending west from the Florida coast in the 10 to 12

295      km region. Figure 5 shows the vertical profile of the lightning $NO_x$ mass as it is

296      introduced into the model domain, as well as its profile following convection from the

297      same simulation as Figure 4. The bimodal distribution of the profile of injected $LNO_x$

298      mass reflects the bimodal distribution of IC flash channel segments calculated by the

299      CSCTM. The upper mode peak is initially smaller in magnitude because the $LNO_x$ is

300      distributed with a dependence on pressure as described in DeCaria et al. [2005]. Upward

301      transport during the storm results in $LNO_x$ originally introduced into the model at

302      altitudes near the lower mode peak residing near the top of the cloud following

303      convection.

304          On July 16, 2002, an isolated convective system developed northwest of Miami

305      shortly after 1900 UTC (1500 LT) and was investigated as part of the CRYSTAL-FACE

306      project. Over the next few hours, the storm moved west across the Florida peninsula and

307      was extensively sampled by the WB-57 from 1936 to 2306 UTC at altitudes ranging from

308      9 to 15.5 km AGL. The storm was simulated using the Advanced Regional Prediction

309      System (ARPS) described in Xue et al. [2000; 2001] with a horizontal resolution of 2 km

310      and vertical resolution varying from 25 m near the surface to 0.5 km near the top of the

311      model domain at approximately 25 km. A number of different types of observations,

312 including radar reflectivity, were assimilated into the simulation. The simulated temporal

313 evolution of the storm matched observations well, as did storm size. The CSCTM was

314 used to calculate the transport of tracer species CO and $O_3$ and a comparison of model

315 results with anvil aircraft observations showed that the model adequately represented

316 transport within the storm.

317      Figure 6 shows the time series of flash rates recorded by the ground-based NLDN

318 from 1900 to 2300 UTC. In contrast to the July 29 CRYSTAL-FACE storm, the July 16

319 storm was a relatively weak lightning producer with only 301 CG flashes recorded during

320 this period and a maximum CG flash rate of 9 flashes per minute. The percentage of

321 weak positive flashes (peak current < 10kA) was calculated during the July 16 storm and

322 was over 20 times greater during the storm than for the month of July as a whole.

323 Because the flash rate during the storm represented too small a sample to reliably make a

324 large adjustment, IC flash rates were estimated from the observed CG flash rates and the

325 climatological IC to CG ratio of 2 for south Florida from Boccippio et al. [2001]. Based

326 on the mean peak current of CG flashes recorded by the NLDN for this storm (23 kA),

327 $P_{CG}$ was estimated to be 700 moles of NO. In this simulation, the upper mode of the IC

328 flash channel distribution was set to -60°C. Several different values of the $P_{IC}/P_{CG}$ ratio

329 were simulated and the results compared with observations. The assumption that on

330 average, an IC flash produces 75% as much NO as a CG flash yielded the most favorable

331 comparison with the column mass of N in $NO_x$ estimated from observations when

332 chemical reactions were not simulated. The simulation of chemistry led to a decrease in

333 $NO_x$ mixing ratios due to conversion of $NO_x$ to reservoir species such as $HNO_3$ and PAN.

334 In order to match aircraft observations, a $P_{IC}/P_{CG}$ ratio of 0.9 was needed. Figure 7 shows

335 a vertical cross-section of $NO_x$ calculated assuming this production scenario taken

336 through the core of the storm after 180 minutes of simulation. Maximum $NO_x$ mixing

337 ratios exceeding 5 ppbv are found at 6.5 km while lower concentrations are found in the

338 upper part of the core and anvil.

339       Figure 8 shows the percentage of the mass of N in $LNO_x$ in each kilometer-deep

340 layer after both the July 16 and 29 CRYSTAL-FACE storms. Following the July 29

341 storm, the maximum in the vertical mass distribution is found at anvil levels (~10 – 11

342 km). In the case of the July 16 storm, the maximum is found in the 6-7 km layer,

343 coincident with the lower mode of the vertical distributions of the $LNO_x$ source in the

344 CSCTM. A smaller peak is found in 9-10 km layer, the height of the upper mode of the

345 distribution, and another peak at 12-13 km, near the top of the cloud. These vertical

346 $LNO_x$ mass distributions are based on the assumed IC to CG ratios of 2 and 5 for the July

347 16 and 29 storms, respectively. Because IC to CG ratios may be highly variable and were

348 estimated for these simulations, the results of a sensitivity test of the assumption of IC to

349 CG ratios of 2 and 5 are shown for the July 16 storm in Figure 9a and for the July 29

350 storm in Figure 9b. For both storms, assuming an IC to CG ratio of 2 results in a slightly

351 larger percentage of $LNO_x$ mass residing in the lower and middle portion of the cloud and

352 a smaller percentage of $LNO_x$ mass near the cloud top (12-14 km for the July 16 case and

353 10-12 km for the July 29 storm).

354 3.2.     Midlatitude Continental Events

355       The STERAO field project was conducted in June and July, 1996 over

356 northeastern Colorado to study lightning $NO_x$ production and convective transport of

357 chemical species. CG lightning activity was monitored by the NLDN, while total

358 lightning activity, including both CG and IC flashes, was mapped by a VHF

359 interferometer. Two storms observed during the STERAO field project were simulated

360 and lightning $NO_x$ production per flash estimated in each. A similar analysis was

361 conducted for one storm from the EULINOX field project conducted in southern

362 Germany in July 1998. The fourth midlatitude storm simulated was from the 1985

363 PRESTORM experiment conducted over Kansas/Oklahoma.

364     All four midlatitude storms were simulated using the 3-D Goddard Cumulus

365 Ensemble (GCE) model, which is described in Tao and Simpson [1993] and Tao et al.

366 [2003a]. A description of the GCE simulation of the July 12 STERAO storm is contained

367 in Stenchikov et al. [2005], while the results of the chemical transport model simulation

368 are found in DeCaria et al. [2005]. Between 2000 and 2400 UTC (1400 and 1800 LT),

369 188 CG flashes and 2121 IC flashes were recorded by the NLDN and interferometer,

370 respectively. Flash counts for the STERAO storms only include interferometer flashes

371 with duration greater than 100 ms. Whether or not short duration flashes, which would

372 not be recorded by some lightning detection systems, are productive of NO is an open

373 question. DeCaria et al. [2005] estimated that $P_{CG}$ was 460 moles NO based on the mean

374 peak current of 15 kA. Assuming that an IC flash was equally as efficient at producing

375 NO as a CG flash yielded the best comparison with observations in terms of mean

376 vertical profile shapes while a $P_{IC}/P_{CG}$ ratio between 0.75 and 1 compared most favorably

377 with observed column mass.

378     On July 10, 1996, a multi-cellular thunderstorm organized in a northwest to

379 southeast line developed near the Wyoming-Nebraska border at approximately 2100 UTC

380 (1500 LT) and was observed as part of the STERAO campaign [Dye et al., 2000;

381 Skamarock et al., 2000; 2003]. Research aircraft investigated the storm from 2237 to

382 0105 UTC. After 0115 UTC, the storm became unicellular with supercell chracteristics.

383 IC lightning activity dominated throughout the lifetime of the storm with only 77 CG

384    flashes and 3223 IC flashes recorded between 2201 and 0206 UTC. The University of

385    North Dakota Citation aircraft observed maximum NO mixing ratios of 1 ppbv

386    approximately 60 km downstream of the storm cores [Dye et al., 2000].

387         The GCE model with a horizontal resolution of 2 km and 0.5 km vertical

388    resolution was used to simulate the July 10 STERAO storm. The GCE and CSCTM

389    simulations were included in a cloud-chemistry model intercomparison study described in

390    Barth et al. [2007]. Both the magnitude and height of the simulated peak updraft velocity

391    compared well with observations. Convective transport was evaluated by comparing

392    simulated CO and $O_3$ mixing ratios with observations obtained during two across-anvil

393    transects. While the simulation underrepresented transport during the first transect,

394    mixing ratios in the later transect were reproduced well by the CSCTM simulation,

395    indicating that convective transport was adequate after an initial spin-up period.

396         Simulated storm speed and cloud top heights compared favorably with radar

397    observations. For the simulations of the July 10 STERAO and July 21 EULINOX

398    storms, the parameterization of $LNO_x$ production was modified to simulate individual

399    flashes. The method is fully illustrated in Ott et al. [2007]. Each flash is simulated by

400    selecting grid cells at random from an area of the domain centered just downwind of the

401    maximum updraft, which is similar in size to the area where lightning flashes typically

402    occurred. The downwind location was chosen based on plots of radar reflectivity and

403    flash location in Höller et al. [2000] and Dye et al. [2000] that show the majority of

404    lightning activity occurring slightly downwind of the core updraft region. The number of

405    grid cells included in a flash at each level is determined by vertical distributions adapted

406    from the Gaussian distributions calculated in the original bulk method of $LNO_x$

407    parameterization described in DeCaria et al. [2005]. Simulations of both the July 10

408   STERAO and July 21 EULINOX storms using both the original and modified $LNO_x$

409   parameterizations show that the difference in parameterization produces little change in

410   the vertical distribution of $LNO_x$ following convection. The upper mode of the IC flash

411   channel distribution was set to -50°C for the July 10 STERAO storm.

412        In the July 10 STERAO storm, $P_{CG}$ was estimated to be approximately 390 moles

413   based on the observed peak current (13 kA) of CG flashes. Assuming a $P_{IC}/P_{CG}$ ratio of

414   0.5 matched in-cloud aircraft observations well when chemical reactions were not

415   considered. When chemical reactions were simulated, the $P_{IC}/P_{CG}$ ratio was increased to

416   0.6 to match observations. Figure 10 shows a vertical cross section of calculated $NO_x$

417   through the core of the southernmost cell in the line of thunderstorms at the end of the

418   180 minute simulation. $NO_x$ mixing ratios exceed 2.8 ppbv at 3.5 km above the surface

419   but are only ~1 ppbv in the anvil region.

420        The EULINOX field project was conducted in central Europe in June and July

421   1998 in order to study lightning $NO_x$ production over Europe. In addition to two research

422   aircraft, the project included observations of CG lightning activity from the ground-based

423   lightning detection system known as BLIDS (Blitz Informationsdienst von Siemens).

424   One storm from the EULINOX project, which occurred on July 21, 1998 over southern

425   Germany, was simulated using the GCE model. The storm developed as a single cell and

426   after an initial period of intensification split into two distinct cells. The northernmost cell

427   became multicellular in structure and was observed to decay rapidly, while the southern

428   cell strengthened and developed supercell characteristics. The southern cell produced

429   360 CG and 2565 IC flashes between 1640 and 1900 UTC (1840 and 2100 LT), while the

430   northern storm produced 289 CG and 815 IC flashes. The GCE simulation succeeded in

431   reproducing a number observed storm features, including the cell-splitting. A full

432    description of the GCE and CSCTM simulations is provided in Ott et al. [2007]. Based

433    on the mean peak current (12 kA) of CG flashes, $P_{CG}$ was estimated to be 360 moles NO.

434    The upper mode of the IC flash channel distribution was set to -45°C in this simulation.

435    Several different values of $P_{IC}$ were simulated, and the scenario in which $P_{IC}$ is equal to

436    $P_{CG}$ was found to compare most favorably with observations, though observed column

437    mass was underestimated by 10%. In order to match observed column mass, the $P_{IC}/P_{CG}$

438    ratio needed to be increased to 1.15.

439        In addition to the STERAO and EULINOX storms, the June 10-11 squall line

440    observed during the PRE-STORM project was simulated using the GCE model. The

441    June 10-11 squall line has been documented extensively [e.g. Johnson and Hamilton,

442    1988; Rutledge et al., 1988] and has previously been simulated using the 2-D version of

443    the GCE [Tao et al., 1993]. In this case, the horizontal resolution of the 3-D GCE was

444    1.5 km and vertical resolution varied from approximately 0.25 km near the surface to

445    slightly more than 1 km near the top of the domain at 21.4 km. During PRE-STORM, the

446    occurrence of CG lightning flashes was recorded by the National Severe Storms

447    Laboratory's Lightning Location Network. Based on a time series of positive and

448    negative CG flash rates from Nielsen et al. [1994], approximately 6500 CG flashes

449    occurred during the storm's lifetime. Observations of total lightning activity were

450    unavailable, so the climatological IC/CG ratio of 3 for the region [Boccippio et al, 2001]

451    was assumed to estimate IC flash rates. The upper mode of the IC flash channel

452    distribution was set to -45°C. No observations of the chemical environment of the squall

453    line anvil are available. Therefore, it was not possible to estimate a production scenario

454    for IC and CG flashes as in the other five storms. Instead, the average value of $P_{CG}$

455     calculated over the five other storms (~500 moles NO per flash) was used along with an

456     estimate of $P_{IC}$ that was 85% of $P_{CG}$ or 425 moles of NO.

457        Figure 11 shows the vertical distribution of the mass of N in $LNO_x$ for the four

458     midlatitude continental storms. The distributions for the four storms all reflect the double

459     peaked distribution of $LNO_x$ produced by IC flashes in the model. There is variation

460     between the simulations in the dominant mode of the lightning distributions. In the

461     EULINOX and PRESTORM storms whose IC to CG ratios were on average 5 and 3,

462     respectively, a higher percentage of $LNO_x$ mass is found near the height of the lower

463     mode of the IC distribution, which is also the mode of the CG distribution. In the July 10

464     and July 12 STERAO storms, which had average IC to CG ratios of 33 and 8 during the

465     time periods simulated, a greater percentage of $LNO_x$ mass resides near the height of the

466     upper mode of the IC vertical distribution following convection. In addition to the IC to

467     CG ratio, the dominance of the modes is likely affected by storm dynamics and the

468     timing of IC and CG flashes in relation to the evolution of the storm.

469     4.       Applications for large-scale models and remote sensing

470     4.1      Vertical distribution of lightning $NO_x$ mass

471        We have presented results from the simulations of six thunderstorms using the 3-

472     D CSCTM. Figure 12a shows the average vertical distribution of the mass of N in $LNO_x$

473     calculated by averaging the case studies in the subtropical regime and Figure 12b shows

474     the average vertical distribution for storms in the midlatitude regime overlaid with the

475     vertical distribution calculated by Pickering et al. [1998]. Both plots are overlaid with

476     smooth curves fit to the regime average. Table 2 lists the percentages of $LNO_x$ mass in

477     each 1-km layer taken from the smoothed curves. In both regimes on average, only a

478     small percentage of $LNO_x$ resides in the boundary layer following the convective event.

479    A greater percentage of $LNO_x$ remains in the middle and upper troposphere where the

480    $LNO_x$ was originally produced. These "backward C-shaped" average vertical

481    distributions are in marked contrast to the C-shaped profiles presented in Pickering et al.

482    [1998] based on 2-D cloud-resolving model simulations where a significant percentage of

483    $LNO_x$ mass was transported to the boundary layer and relatively little $LNO_x$ mass was

484    found between 1.5 and 6.5 km after convection concluded. Our results are similar to

485    those from recent 3-D cloud models with explicit electrophysics. For example, Zhang et

486    al. [2003a] found a maximum in $NO_x$ at mid-levels along with a secondary maximum at

487    anvil levels indicating that a large portion of the $LNO_x$ remains within the cloud near the

488    levels of its production. It should also be noted that our simulations indicate a small

489    percentage of mass (~1%) remains above the tropopause following convection, which

490    results from overshooting transport of lightning $NO_x$ produced at lower altitudes.

491    Individual modeling groups who implement these profiles may want to consider scaling

492    these profiles so that mass is not directly injected into the stratosphere because most

493    convective parameterizations used in larger-scale models do not produce overshooting

494    cloud tops. Implementation of the profiles should involve scaling them to calculated

495    cloud top height on an individual grid cell basis.

496          Assuming the density profile of the standard atmosphere, the total mass of

497    lightning $NO_x$ was averaged over the EULINOX and STERAO storms. That amount of

498    $NO_x$ distributed uniformly over a 200 km by 200 km region (typical of a global model

499    grid cell) using the average midlatitude profile shown in Table 2 corresponds to a

500    maximum increase in $NO_x$ mixing ratios of ~ 145 pptv between 7 and 9 km immediately

501    following convection (~2 km higher than the maximum of the lightning $NO_x$ mass

502    distribution). Because the lifetime of $NO_x$ increases with altitude, lightning $NO_x$ will be

503  converted to reservoir species such as PAN and $HNO_3$ more rapidly in the 7-9 km layer

504  than at higher altitudes. As the time after convection increases, the maximum increase in

505  $NO_x$ mixing ratios due to lightning would be seen at higher altitudes, which is consistent

506  with the C-shaped profile of $NO_x$ typically observed in the troposphere. Downward

507  transport from the stratosphere also contributes to the upper tropospheric maximum in

508  observed $NO_x$ mixing ratios, while the maximum near the surface results from emissions

509  from surface sources such as fossil fuel combustion and soil.

510      The impact of assuming the vertical distributions of lightning $NO_x$ mass presented

511  here has been calculated using NASA's Global Modeling Initiative (GMI) combined

512  stratosphere-troposphere (Combo) CTM. The Combo CTM is detailed in Ziemke et al.

513  [2006] and Duncan et al. [2007]. The tropospheric chemical mechanism includes 80

514  species and 300 reactions to simulate $O_3$-$NO_x$-hydrocarbon chemistry [Bey et al. 2001].

515  Lightning is assumed to produce 5 TgN $yr^{-1}$. Horizontal distribution of lightning $NO_x$ is

516  determined by the locations of parameterized deep convection (as indicated by the upper

517  tropospheric values of cloud mass flux) in the meteorological fields from the Global

518  Modeling and Assimilation Office's GEOS-4 Data Assimilation System that are used to

519  drive the Combo CTM. Flash rates are scaled such that on a regional and monthly basis

520  they match those from the OTD/LIS climatology (Allen et al., 2009).

521      Two one-year simulations were produced by the Combo CTM. The first used the

522  vertical profiles of lightning $NO_x$ from Pickering et al. [1998] while the second

523  simulation used the vertical profiles of lightning $NO_x$ shown in Figure 12a and b for the

524  midlatitude and subtropical regimes. Because no tropical thunderstorms were simulated

525  with the cloud and chemistry models, a hypothetical tropical distribution (Figure 12c)

526  was constructed by extrapolating the subtropical profile to a higher tropopause regime.

527    Test runs of the GMI Combo CTM revealed that this profile performed well in regions

528    dominated by marine convection, but in tropical continental areas the Pickering et al.

529    [1998] profile yielded better results for upper tropospheric ozone compared with

530    ozonesonde data. Therefore, in tropical continental regions the Pickering et al. [1998]

531    profile, modified by removing the boundary layer maximum and redistributing this mass

532    between 4 and 11 km, was used. The tropical profiles are also provided in Table 2.

533        Figure 13 shows the zonal mean change in $NO_x$ and $O_3$ in January and July when

534    the profiles shown in Figure 12 are used instead of the Pickering et al. [1998] profiles.

535    Because these profiles place less NO in the upper troposphere, $NO_x$ decreases above 10

536    km with decreases over 100 pptv found over the southern hemisphere in January and over

537    the northern hemisphere in July. The decrease in $NO_x$ in the upper troposphere, which

538    results from using the modified vertical profiles of lightning $NO_x$ mass, also causes a

539    small decrease in ozone throughout much of the troposphere. The largest decrease in

540    ozone is ~10 ppbv in July at 15 km and 30°N.

541    4.2.    NO production

542        A best-fit production scenario of $P_{IC}$ and $P_{CG}$ has been estimated by comparing in-

543    cloud aircraft observations with model output for the five storms where in-cloud aircraft

544    observations were available. Figure 14 shows the production scenarios estimated for

545    these five storms as well as the production scenario from Price et al. [1997], which was

546    used in calculating the vertical profiles of $LNO_x$ mass presented in Pickering et al. [1998]

547    and has been used in many global CTMs. In all cases, $P_{CG}$ was estimated to be less than

548    the 1100 moles per CG flash given in Price et al. [1997]. In addition, in all cases the ratio

549    of $P_{IC}$ to $P_{CG}$ was greater than the commonly assumed value of 0.1 presented by Price et

550    al. [1997]. Over the five storms simulated, the average estimated $P_{CG}$ was 500 moles NO

551    per flash or 7 kg N per flash (range of 360 to 700 moles per flash or ~5 to 9.8 kg N per

552    flash). Assuming $P_{IC}/P_{CG}$ ratios in the middle of the estimated uncertainty ranges for the

553    July 29 CRYSTAL-FACE, July 12 STERAO, and July 21 EULINOX storms yields an

554    average $P_{IC}/P_{CG}$ ratio of 0.93, corresponding to 465 moles NO. The median peak current

555    (16.5 kA for negative flashes and 19.8 kA for positive flashes, which account for 10.9%

556    of the total) of the North American Lightning Detection Network (NALDN) presented in

557    Orville et al. [2002] corresponds to a $P_{CG}$ value of 508 moles NO when using the Price et

558    al. [1997] relationship between peak current and energy dissipated, which agrees well

559    with our estimate of 500 moles NO per CG flash. Therefore, the cases we have simulated

560    appear to be representative of midlatitude and subtropical lightning. Assuming the

561    average production scenario over the five storms presented, an average global IC to CG

562    ratio of 3 (the same as estimated for the continental United States by Boccippio et al.,

563    2001) , and a global flash rate of 44 flashes $s^{-1}$ [Christian et al., 2003] yields a global

564    lightning NO source of 8.6 Tg N $yr^{-1}$.

565          Estimates of the global lightning NO source have ranged from 2-20 Tg N $yr^{-1}$

566    [IPCC, 2001]. This range has been narrowed in recent years. IPCC [2007] recommends

567    a 1.1-6.4 Tg N $yr^{-1}$ range, though a more comprehensive review has specified the range to

568    be 2-8 Tg N $yr^{-1}$ [Schumann and Huntrieser, 2007]. This review considered all of the

569    methods of estimating $LNO_x$ production: global model estimates constrained by various

570    observations, cloud-resolved modeling studies, aircraft measurements, laboratory

571    experiments, and theoretical estimates. Our estimate of 8.6 Tg N $yr^{-1}$ lies near the upper

572    end of the recently established range of global estimates. It is unlikely that our estimate

573    is larger than values in this range due to the global extrapolation. Because of satellite

574    observations of total lightning activity from instruments such as the Optical Transient

575     Detector (OTD; see Christian et al., 2003), uncertainty in the global flashrate has been

576     greatly reduced. Perhaps more likely it is due to the fact that our average production

577     scenario was calculated using data from only midlatitude continental and subtropical

578     storms. No tropical thunderstorms were simulated in this analysis. Because 78% of

579     lightning flashes occur between 30°S and 30°N [Christian et al., 2003], further

580     investigation of the properties of tropical lightning flashes and their production of NO is

581     needed. Based on analysis of data from the TROCCINOX experiment in Brazil,

582     Huntrieser et al. [2008] suggest that tropical flashes (shorter, possibly due to low vertical

583     wind shear) produce less $LNO_x$ than subtropical or midlatitude flashes (longer, possibly

584     due to greater wind shear). If this hypothesis holds true throughout the tropics, inclusion

585     of tropical events into our average production scenario will decrease this average value.

586     Tropical event simulations are currently underway.

587        Several modeling studies have assumed a production scenario similar to the mean

588     scenario presented here where both IC and CG flashes produce on average approximately

589     500 moles NO per flash. Hudman et al. [2007] simulated $NO_x$ over the United States

590     during the ICARTT campaign using the GEOS-Chem CTM and found that assuming a

591     production per flash of 500 moles NO instead of the default GEOS-Chem value of 125

592     moles NO improved the comparison with upper tropospheric aircraft observations.

593     Cooper et al. [2006] simulated $LNO_x$ production and transport over North America

594     during the same period using the FLEXPART model and assumed IC and CG flashes

595     produce 460 moles NO (based on the DeCaria et al. [2005] results for the July 12

596     STERAO storm) and a 2-day lifetime for upper tropospheric $NO_x$. Resulting ozone

597     enhancements were estimated with a box model. The results showed a good agreement

598     between simulated $NO_x$ and DC-8 aircraft observations and between simulated ozone

599   enhancements and observations from commercial aircraft and ozonesondes.  Jourdain et

600   al. [2009] found that assuming a production per flash of 520 moles NO (rather than 260

601   moles NO) in GEOS-Chem simulations of ozone over the United States substantially

602   reduced the model's bias relative to TES observations.  Choi et al. [2008] compared

603   results from a regional CTM with tropospheric $NO_2$ columns from OMI and tropospheric

604   $O_3$ columns derived from a combination of OMI and MLS data and found that the model,

605   assuming IC and CG flashes produce 500 moles NO, was able to reasonably reproduce

606   the spatial distribution of the satellite observations.

607   4.3     $NO_2$ in the vicinity of electrified storms

608           $NO_2$ profiles appropriate for regions dominated by $NO_x$ from lightning are useful

609   for improving satellite retrievals of $NO_2$ column amounts in such environments.  The air

610   mass factor used in converting satellite-measured slant columns to vertical columns of

611   $NO_2$ is highly dependent on the $NO_2$ profile shape.  $NO_2$ profiles from the version of the

612   CSCTM that includes chemical production and loss have been used to examine the

613   structure of this species in the CRYSTAL-FACE, STERAO, and EULINOX storms.

614           Mean vertical profiles of $NO_2$ after convection are shown in Figure 15.  The

615   profiles were calculated over a 40 by 40 km area positioned in the convective core region

616   of the model domain.  The July 29 profile shows extremely elevated $NO_2$ mixing ratios

617   exceeding 2 ppbv from 5 to 7.5 km, while the July 16 profile maximizes at only 0.7 ppbv

618   at 9.5 km.  The disparity in profiles is due to the large difference in flash rates in the two

619   storms with over 4000 CG flashes recorded by the NLDN in the July 29 storm, and only

620   301 CG flashes recorded in the July 16 storm.  Of the midlatitude storms, the vertical

621   profile of $NO_2$ from the EULINOX storm (with both high flash rate and pollution inflow)

26

622    is much larger than in either of the STERAO storms with a maximum of nearly 3 ppbv at

623    5.5 km.

624        In addition to $NO_2$ profiles, we have also used these simulations to estimate

625    partial columns of $NO_2$ that a satellite may be able to observe in the upper portion of a

626    convective cloud. Vasilkov et al. [2008] compared cloud-top pressures retrieved in the

627    UV wavelengths by the Ozone Monitoring Instrument (OMI) aboard the Aura satellite

628    with those retrieved by IR measurements from MODIS aboard Aqua. A comparison of

629    both cloud-top pressure products with CloudSat radar observations indicate that OMI

630    may be able to measure $NO_2$ as far down as 400 to 600 mb in the presence of deep

631    convective clouds. Partial $NO_2$ columns were calculated for our storms of interest by

632    averaging 2-km model output over 13 km by 24 km areas equivalent to OMI's nadir

633    footprint and integrating the column from 400 mb to the tropopause. The results are

634    shown in Figure 16. The July 29 CRYSTAL-FACE and July 21 EULINOX storms show

635    the greatest degree of enhancement, which is consistent with the $NO_2$ profiles shown in

636    Figure 15. In the July 29 CRYSTAL-FACE storm, the region of highly elevated $NO_2$

637    columns extends over 100 km. Table 3 shows the sensitivity of the peak and background

638    $NO_2$ columns to the choice of column depth. The peak values indicate the maximum

639    partial $NO_2$ column amounts over an OMI grid box area (13 km by 24 km) in the storm

640    anvil or core regions, while the background values indicate the mean partial $NO_2$ column

641    amounts outside of the storm region. These data should be useful in providing a range of

642    values of tropospheric column $NO_2$ that may be compared to retrievals over convective

643    clouds from such instruments as OMI.

644    5.    Conclusions

645        Simulations of six midlatitude and subtropical thunderstorms occurring during

646    four field projects have been conducted using the CSCTM, which includes a

647    parameterized source of $LNO_x$. In order to estimate $LNO_x$ production per flash in each

648    storm, different scenarios of $P_{IC}$ and $P_{CG}$ were specified in the model, and the results

649    compared with in-cloud aircraft observations of $NO_x$. By comparing column mass and

650    probability distribution functions of the observed and simulated storms, the most

651    appropriate production scenario was estimated for each storm. The results suggest that

652    $P_{IC}$ may be nearly the same as $P_{CG}$. A frequent assumption that $P_{IC}$ is equal to one tenth

653    $P_{CG}$ resulted in a significant underestimation of $LNO_x$ in all five simulations where anvil

654    observations were available. We echo the recommendation of Ridley et al. [2005] for use

655    of comparable values of $P_{CG}$ and $P_{IC}$. The Ridley et al. [2005] recommendation was

656    partly based on one of the cases presented here. Our similar results for four additional

657    cases strengthen this recommendation. The mean $P_{CG}$ obtained from the five case

658    simulations is 500 moles NO per flash (range 360 to 700), which, when extrapolated

659    globally, yields an estimate at the high end of the currently accepted range. This may

660    result from the absence of tropical flashes in this analysis.

661        Vertical profiles of the percentage of $LNO_x$ mass in each 1-km layer after the

662    convection show very little $LNO_x$ mass near the surface with the majority of $LNO_x$

663    remaining in the mid- and upper troposphere in a "backward C-shaped" profile. Global

664    and regional CTMs that have adopted C-shaped vertical profiles of $LNO_x$ mass may be

665    underestimating the amount of $LNO_x$ in the mid- troposphere and overestimating the

666    amount near the surface. Global models which are changed to represent equivalent per

667    flash production by IC and CG lightning may require a change of the global $LNO_x$ source

668    strength to reasonably reproduce $NO_x$ observations in the middle and upper troposphere.

669     Changes in the vertical placement of $LNO_x$ in CTMs may significantly alter distributions

670     of species such as $O_3$ and OH.

671

679
680     References
681

682     Allen, D. J., and K. E. Pickering (2002), Evaluation of lightning flash rate
683     parameterizations for use in a global chemical-transport model , *J. Geophys. Res.*,
684     *107*(D23), 4711,doi:10.1029/2002JD002066.

685
686     Allen, D. J., K. E. Pickering, J. Rodriguez, B. Duncan, S. Strahan, and M. Damon
687     (2009), Impact of lightning-NO emissions on North American photochemistry as
688     determined using the GMI model, in preparation for *J. Geophys. Res.*

689
690     Barth, M. C., S.-W. Kim, C. Wang, K. E. Pickering, L.E. Ott, G. Stenchikov, M. Leriche,
691     S. Cautenet, J.-P. Pinty, C. Barthe, C. Mari, J. H. Helsdon, R. D. Farley, A. M. Fridlind,
692     A. S. Ackerman, V. Spiridonov, and B. Telenta (2007), Cloud-scale model
693     intercomparison of chemical constituent transport in deep convection, *Atmos. Chem.*
694     *Phys.*, *7*, 4709-4731.

695
696     Beirle, S., N. Spichtinger, A. Stohl, K. L. Cummins, T. Turner, D. Boccippio, O. R.
697     Cooper, M. Wenig, M. Grzegorski, U. Platt, and T. Wagner (2006), Estimating the $NO_x$
698     produced by lightning from GOME and NLDN data: a case study in the Gulf of Mexico,
699     *Atmos. Chem. Phys.*, *6*, 1075-1089.

700
701     Bey, I., D. J. Jacob, R. M. Yantosca, J. A. Logan, B. D. Field, A. M. Fiore, Q. Li, H. Y.
702     Liu, L. J. Mickley, and M. G. Schultz (2001), Global modeling of tropospheric chemistry
703     with assimilated meteorology: Model description and evaluation, *J. Geophys. Res.*,
704     *106*(D19), 23,073–23,095.
705

706  Boccippio, D. J., K. L. Cummins, H. J. Christian, and S. J. Goodman (2001), Combined
707  satellite- and surface-based estimation of the intracloud–cloud-to-ground lightning ratio
708  over the continental United States, *Monthly Weather Review, 129*, 108–122.
709
710  Boersma, K. F., H. J. Eskes, E. W. Meijer, and H. M. Kelder (2005), Estimates of
711  lightning NOx production from GOME satellite observations, *Atmos. Chem. Phys., 5*,
712  2311-2331.
713
714  Christian, H.J., et al. (2003), Global frequency and distribution of lightning as observed
715  from space by the Optical Transient Detector, *J. Geophys. Res., 108*(D1), 4005,
716  doi:10.1029/2002JD002916
717
718  Choi, Y., A. Eldering, G. Osterman, Y. Wang, D. Cunnold, Q. Yang, E. Bucsela, and K.
719  E. Pickering (2008), Lightning and anthropogenic NOx sources over the U.S. and the
720  western North Atlantic Ocean: 1. Impact on tropospheric $O_3$ from space-borne
721  observations, submitted to *J. Geophys. Res.*
722
723  Cooper, O. R., et al. (2006), Large upper tropospheric ozone enhancements above
724  midlatitude North America during summer: In situ evidence from the IONS and
725  MOZAIC ozone measurement network, *J. Geophys. Res., 111*, D24S05,
726  doi:10.1029/2006JD007306.
727
728  Cummins, K. L., M. J. Murphy, E. A. Bardo, W. L. Hiscox, R. B. Pyle, and A. E. Pifer
729  (1998), A Combined TOA/MDF Technology Upgrade of the U.S. National Lightning
730  Detection Network, *J. Geophys. Res., 103*, 9035-9044.
731
732  DeCaria, A. J., K. E. Pickering, G. L. Stenchikov, J. R. Scala, J. L. Stith, J. E. Dye, B. A.
733  Ridley, and P. Laroche (2000), A cloud-scale model study of lightning-generated $NO_x$ in
734  an individual thunderstorm during STERAO-A, *J. Geophys. Res., 105*, 11,601-11,616.
735
736  DeCaria, A. J., K. E. Pickering, G. L. Stenchikov, and L. E. Ott (2005), Lightning-
737  generated $NO_x$ and its impact on tropospheric ozone production: A three-dimensional
738  modeling study of a Stratosphere-Troposphere Experiment: Radiation, Aerosols, and
739  Ozone (STERAO-A) thunderstorm, *J. Geophys. Res., 110*, D14303,
740  doi:10.1029/2004JD005556.
741
742  Duncan, B. N., S. E. Strahan, Y. Yoshida, S. D. Steenrod, and N. Livesey (2007), Model
743  study of the cross-tropopause transport of biomass burning pollution, *Atmos. Chem.
744  Phys., 7*, 3713-3736.
745
746  Dye, J. E., et al., (2000), An Overview of the STERAO--Deep Convection Experiment
747  with Results for the 10 July Storm, *J. Geophys. Res., 105*, 10,023-10,045.
748
749  Fehr, T., H. Höller, H. Huntrieser, Model study on production and transport of lightning-
750  produced $NO_x$ in a EULINOX supercell storm (2004), *J. Geophys. Res., 109*, D09102,
751  doi:10.1029/2003JD003935.
752

753 Gallardo, L., and V. Cooray (1996), Could cloud-to-cloud discharges be as effective as
754 cloud-to-ground discharges in producing $NO_X$?, *Tellus, 48B*, 641-651.
755
756 Höller, H., H. Huntrieser, C. Feigl, C. Théry, P. Laroche, U. Finke, and J. Seltmann
757 (2000), The Severe Storms of 21 July 1998 – Evolution and Implications for $NO_X$-
758 Production, in *EULINOX – The European Lightning Nitrogen Oxides Experiment*, edited
759 by H. Höller and U. Schumann, *Rep. DLR-FB 2000-28*, pp. 109-128, Deutches Zentrum
760 für Luft- und Raumfahrt, Köln.
761
762 Holmes, C., M. Brook, P. Krehbiel, and R. McRory (1971), On the power spectrum and
763 mechanism of thunder, *J. Geophys. Res., 76,* 2106-2115.
764
765 Hudman, R. C., et al. (2007), Surface and lightning sources of nitrogen oxides over the
766 United States: Magnitudes, chemical evolution, and outflow, *J. Geophys. Res., 112,*
767 D12S05, doi:10.1029/2006JD007912.
768
769 Huntrieser, H., H. Schlager, C. Feigl, and H. Höller (1998), Transport and production of
770 $NO_X$ in electrified thunderstorms: Survey of previous studies and new observations at
771 mid-latitudes, *J. Geophys. Res., 103,* 28,247-28,264.
772
773 Huntrieser, H., et al., (2002), Airborne measurements of NOx, tracer species, and small
774 particles during the European Lightning Nitrogen Oxides Experiment, *J. Geophys. Res.,*
775 *107*(D11), 4113, doi:10.1029/2000JD000209.
776
777 Huntrieser, H., U. Schumann, H. Schlager, H. Höller, A. Giez, H.-D. Betz, D. Brunner,
778 C. Forster, O. Pinto Jr., and R. Calheiros (2008), Lightning activity in Brazilian
779 thunderstorms during TROCCINOX: implications for NOx production, *Atmos. Chem.*
780 *Phys., 8,* 921-953, 2008.
781
782 IPCC (2001), *Climate Change 2001: The Scientific Basis. Contribution of Working*
783 *Group I to the Third Assessment Report of the Intergovernmental Panel on Climate*
784 *Change.* J. T. Houghton et al., Eds., Cambridge University Press, 892 pp.
785
786 IPCC (2007), *Climate Change 2007: Synthesis Report. Contribution of Working Group I*
787 *to the Fourth Assessment Report of the Intergovernmental Panel on Climate Change* S.
788 Solomon et al. (eds.) Cambridge University Press, 996 pp.
789
790 Johnson, R. H., and P. J. Hamilton (1988), The relationship of surface pressure features
791 to the precipitation and airflow structure of an intense midlatitude squall line. *Mon. Wea.*
792 *Rev., 116,* 1444–1472.
793
794 Jourdain, L., S. S. Kulawik, H. M. Worden, K. E. Pickering, J. Worden, and A. M.
795 Thompson, (2009), Lightning NOx emissions over the USA investigated using TES,
796 NLDN, LRLDN, IONS data and the GEOS-Chem model, *Atmos. Chem. Phys. Discuss.,*
797 9, 1123-1155.
798

31

799    Labrador, L. J., R. von Kuhlmann, and M. G. Lawrence, (2004), Strong sensitivity of the
800    global mean OH concentration and the tropospheric oxidizing efficiency to the source of
801    NOx from lightning, *Geophys. Res. Lett.*, *31*(6), L06102, doi:10.1029/2003GL019,229.
802
803    Labrador, L. J., R. von Kuhlmann, and M. G. Lawrence, (2005), The effects of lightning-
804    produced NOx and its vertical distribution on atmospheric chemistry: sensitivity
805    simulations with MATCH-MPIC, *Atmospheric Chemistry and Physics, 5*, 1815-1834.
806
807    Lee D.S., I. Köhler, E. Grobler, F. Rohrer, R. Sausen, L. Gallardo-Klenner, J. G. J.
808    Olivier, F. J. Dentener, and A. F. Bouwman (1997), Estimations of global NOx emissions
809    and their uncertainties, *Atmospheric Environment, 31*:12, 1735-1749.
810
811    Levy, H. II, W. J. Moxim, and P. Kasibhatla (1996), A global three-dimensional time-
812    dependent lightning source of tropospheric $NO_x$. *Journal of Geophysical Research,*
813    *101*(D17), 22,911-22,922.
814
815    Lopez, J. P., et al. (2006), CO signatures in subtropical convective clouds and anvils
816    during CRYSTAL-FACE: An analysis of convective transport and entrainment using
817    observations and a cloud-resolving model, *J. Geophys. Res.*, *111*, D09305,
818    doi:10.1029/2005JD006104.
819
820    MacGorman, D. R., and W. D. Rust (1998), *The Electrical Nature of Storms.* Oxford
821    University Press, 422 pp.
822
823    Madronich, S. (1987), Photodissociation in the Atmosphere 1. Actinic Flux and the
824    Effects of Ground Reflections and Clouds, *J. Geophys. Res., 92*(D8), 9740–9752.
825
826    Maggio, C., T. Marshall, and M. Stolzenburg (2008), Energy estimates for lightning
827    flashes, *EOS Trans. AGU*, 89(53) Fall Meeting Suppl., Abstract AE11A-0294.
828
829    Nielsen, K. E., R. A. Maddox, S.V.Vasiloff (1994), The Evolution of Cloud-to-Ground
830    Lightning within a Portion of the 10–11 June 1985 Squall Line, *Monthly Weather*
831    *Review, 122*, 1809-1817.
832
833    Orville, R. E., G. R. Huffines, W. R. Burrows, R. L. Holle, and K. L. Cummins (2002),
834    The North American Lightning Detection Network (NALDN) - First Results: 1998-2000.
835    *Mon. Wea. Rev., 130, 8*, 2098-2109.
836
837    Ott, L. E., K. E. Pickering, G. L. Stenchikov, H. Huntrieser, and U. Schumann (2007),
838    Effects of lightning NOx production during the 21 July European Lightning Nitrogen
839    Oxides Project storm studied with a three-dimensional cloud-scale chemical transport
840    model, *J. Geophys. Res., 112*, D05307, doi:10.1029/2006JD007365.
841
842    Pickering, K. E., Y. Wang, W.-K. Tao, C. Price, and J.-F. Müller (1998), Vertical
843    distributions of lightning NOx for use in regional and global chemical transport models.
844    *J. Geophys. Res., 103*, 31,203-31,216.
845

846  Price, C., J. Penner, and M. Prather, NOx from lightning (1997), 1, Global distributions
847  based on lightning physics, *J. Geophys. Res.*, *102*, 5929-5941.
848
849  Rahman, M., V. Cooray, V. A. Rakov, M. A. Uman, P. Liyanage, B. A. DeCarlo, J.
850  Jerauld, and R. C. Olsen III (2007), Measurements of NOX produced by rocket-triggered
851  lightning, *Geophys. Res. Lett.*, *34*, L03816, doi:10.1029/2006GL027956.
852
853  Ridley, B., et al. (2004), Florida thunderstorms: A faucet of reactive nitrogen to the upper
854  troposphere, *J. Geophys. Res.*, 109, D17305, doi:10.1029/2004JD004769.
855
856  Ridley B., K. Pickering and J. Dye, (2005), Comments on the parameterization of
857  lightning-produced NO in global chemistry-transport models, *Atmos. Environ.*, *39*, 6184-
858  6187.
859
860  Rutledge, S. A. and D. R. MacGorman (1988), Cloud-to- ground lightning activity in the
861  10-11 June 1985 mesoscale convective system observed during the Oklahoma-Kansas
862  PRE-STORM project, *Mon. Wea. Rev.*, *116,* 1393-1408.
863
864  Rutledge, S. A., R. A. Houze Jr., M. I. Biggerstaff, and T. Matejka (1988), The
865  Oklahoma–Kansas mesoscale convective system of 10–11 June 1985: Precipitation
866  structure and single-Doppler radar analysis, *Mon. Wea. Rev.*, *116,* 1409–1430.
867
868  Schumann, U. and H. Huntrieser (2007), The global lightning-induced nitrogen oxides
869  source, *Atmos. Chem. Phys.*, *7*, 3823-3907.
870
871  Skamarock, W. C., et al. (2000), Numerical simulations of the July 10 Stratospheric-
872  Tropospheric Experiment: Radiation, Aerosols, and Ozone/Deep Convection Experiment
873  convective system: Kinematics and transport, *J. Geophys. Res.*, 105(D15), 19,973–
874  19,990.
875
876  Skamarock, W. C., J. E. Dye, E. Defer, M. C. Barth, J. L. Stith, B. A. Ridley, and K.
877  Baumann (2003), Observational- and modeling-based budget of lightning-produced $NO_x$
878  in a continental thunderstorm, *J. Geophys. Res.*, *108*(D10), 4305,
879  doi:10.1029/2002JD002163.
880
881  Stamnes, K., S.-C. Tsay, W. Wiscombe, and K. Jayaweera (1988), Numerically stable
882  algorithm for discrete-ordinate method radiative transfer in multiple scattering and
883  emitting layered media, *Appl. Opt.*, *27*, 2502-2509.
884
885  Stenchikov, G. L., K. Pickering, A. DeCaria, W.-K. Tao, J. Scala, L. Ott, D. Bartels, and
886  T. Matejka (2005), Simulation of the fine structure of the 12 July 1996 Stratosphere-
887  Troposphere Experiment: Radiation, Aerosols and Ozone ( STERAO-A) storm
888  accounting for effects of terrain and interaction with mesoscale flow, *J. Geophys. Res.*,
889  *110*, D14304, doi:10.1029/2004JD005582.
890
891  Stockwell, D. Z., C. Giannakopoulos, P.-H. Plantevin, G. D. Carver, M. P. Chipperfield,
892  K. S. Law, J. A. Pyle, D. E. Shallcross and K.-Y. Wang (1999), Modelling NOx from
893  lightning and its impact on global chemical fields, *Atmos. Environ.*, *33*, 4477-4493.

894
895    Tao, W.-K., and J. Simpson (1993), Goddard Cumulus Ensemble Model. Part I: Model
896    description, *Terr., Atmos., Oceanic Sci.*, *4*, 35-72.
897
898    Tao, W.-K., J. Simpson, D. Baker, S. Braun, M.-D. Chou, B. Ferrier, D. Johnson, A.
899    Khain, S. Lang, B. Lynn, C.-L. Shie, D. Starr, C.-H. Sui, Y. Wang and P. Wetzel (2003a),
900    Microphysics, Radiation and Surface Processes in the Goddard Cumulus Ensemble
901    (GCE) Model, *Meteorology and Atmospheric Physics, 82,* 97-137.
902
903    Tao, W.-K., et al. (2003b), Regional-scale modeling at NASA Goddard Space Flight
904    Center, *Research Signpost - Recent Res. Devel. Atmos. Sci., 2,* 1-52.
905
906    Vasilkov, A., J. Joiner, R. Spurr, P. K. Bhartia, P. Levelt, and G. Stephens (2008),
907    Evaluation of the OMI cloud pressures derived from rotational Raman scattering by
908    comparisons with other satellite data and radiative transfer simulations, *J. Geophys. Res.,*
909    *113*, D15S19, doi:10.1029/2007JD008689.
910
911    Wang, Y., A. W. DeSilva, G. C. Goldenbaum, and R. R. Dickerson (1998), Nitric oxide
912    production by simulated lightning: Dependence on current, energy, and pressure, J.
913    *Geophys. Res., 103*(D15), 19,149–19,159.
914
915    Xue, M., K. K. Droegemeier, and V. Wong (2000), The Advanced Regional Prediction
916    System (ARPS) - A multiscale non-hydrostatic atmospheric simulation and prediction
917    tool. Part I: Model dynamics and verification, *Meteor. Atmos. Physics., 75,* 161-193.

918

919    Xue, M., K. K. Droegemeier, V. Wong, A. Shapiro, K. Brewster, F. Carr, D. Weber, Y.
920    Liu, and D.-H. Wong (2001), The Advanced Regional Prediction System (ARPS) - A
921    multiscale non-hydrostatic atmospheric simulation and prediction tool. Part II: Model
922    physics and applications, *Meteor. Atmos. Physics., 76,* 134-165.

923
924    Zhang, X., J. H. Helsdon Jr., and R. D. Farley (2003a), Numerical modeling of lightning-
925    produced NO $_x$ using an explicit lightning scheme: 2. Three-dimensional simulation and
926    expanded chemistry, *J. Geophys. Res., 108*(D18), 4580, doi:10.1029/2002JD003225.
927
928    Zhang, X., J. H. Helsdon Jr., and R.D. Farley (2003b), Numerical modeling of lightning-
929    produced $NO_x$ using an explicit lightning scheme: 1. Two-dimensional simulation as a
930    "proof of concept", *J. Geophys. Res., 108*(D18), 4579, doi:10.1029/2002JD003224.
931
932    Ziemke, J. R., S. Chandra, B. N. Duncan, L. Froidevaux, P. K. Bhartia, P. F. Levelt, and
933    J. W. Waters (2006), Tropospheric ozone determine from Aura OMI and MLS:
934    Evaluation of measurements and comparison with the Global Modeling Initiative's
935    chemistry transport model, *J. Geophys. Res., 111*(D19), D19303.
936
937

937    Table 1.  Calculated column mass of N in $NO_x$ in the July 29 CRYSTAL-FACE storm,
938    assuming an IC/CG ratio of 5
939

| $P_{CG}$ (moles NO per flash) | $P_{IC}/P_{CG}$ (IC/CG = 5) | $P_{IC}/P_{CG}$ (IC/CG = 2) | Column Mass (g N m$^{-2}$) |
|---|---|---|---|
| 590 | 0.1 | 0.25 | $2.3 \times 10^{-4}$ |
| 590 | 0.5 | 1.3 | $6.0 \times 10^{-4}$ |
| 590 | 0.6 | 1.5 | $6.9 \times 10^{-4}$ |
| 590 | 0.75 | 1.9 | $8.3 \times 10^{-4}$ |
| 590 | 1.0 | 2.5 | $1.0 \times 10^{-3}$ |

940

940    Table 2. Average Profiles of LNO$_x$ Mass in Percent
941

| Altitude Range, km | Subtropical | Midlatitude | Tropical Continental | Tropical Marine |
|---|---|---|---|---|
| 0-1 | 1.0 | 2.4 | 0.2 | 0.6 |
| 1-2 | 2.1 | 5 | 0.5 | 1.5 |
| 2-3 | 3.9 | 7.4 | 0.6 | 2.9 |
| 3-4 | 5.8 | 9.3 | 1.4 | 4.3 |
| 4-5 | 7.7 | 10.6 | 2.7 | 5.4 |
| 5-6 | 9.3 | 11.4 | 4 | 6.7 |
| 6-7 | 10.5 | 11.5 | 5 | 7.7 |
| 7-8 | 11.0 | 11 | 6.2 | 8.5 |
| 8-9 | 11.0 | 9.9 | 8.6 | 9.6 |
| 9-10 | 10.4 | 8.3 | 10.3 | 10.2 |
| 10-11 | 9.2 | 6.3 | 11.6 | 10.5 |
| 11-12 | 7.5 | 4.2 | 12.4 | 10.2 |
| 12-13 | 5.5 | 2.2 | 12.7 | 8.2 |
| 13-14 | 3.4 | 0.5 | 12.4 | 6.5 |
| 14-15 | 1.5 | 0 | 7.6 | 4.5 |
| 15-16 | 0.2 | 0 | 3.0 | 2.2 |
| 16-17 | 0 | 0 | 0.8 | 0.5 |

942

943
944

945

945     Table 3. Partial $NO_2$ columns ($10^{14}$ molecules $cm^{-2}$) from the tropopause to 400, 500 and
946     600 mb
947
948

| Storm | Tropopause to 400 mb | | Tropopause to 500 mb | | Tropopause to 600 mb | |
|---|---|---|---|---|---|---|
| | Peak | Background | Peak | Background | Peak | Background |
| July 16 CRY | 33 | 1 | 48 | 1 | 54 | 2 |
| July 29 CRY | 104 | 3 | 159 | 3 | 223 | 4 |
| July 10 STE | 13 | 1 | 21 | 1 | 40 | 1 |
| July 12 STE | 21 | 4 | 24 | 5 | 24 | 5 |
| July 21 EUL | 90 | 14 | 140 | 16 | 192 | 17 |

949
950
951
952
953
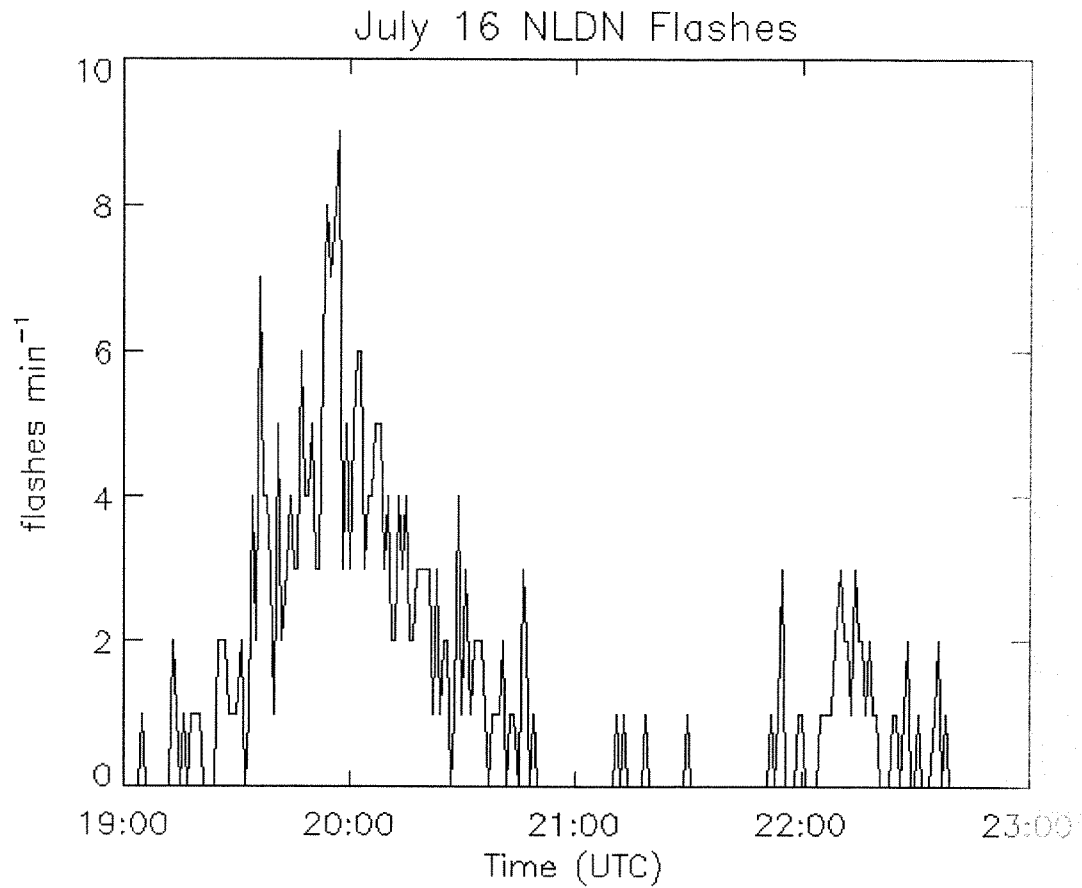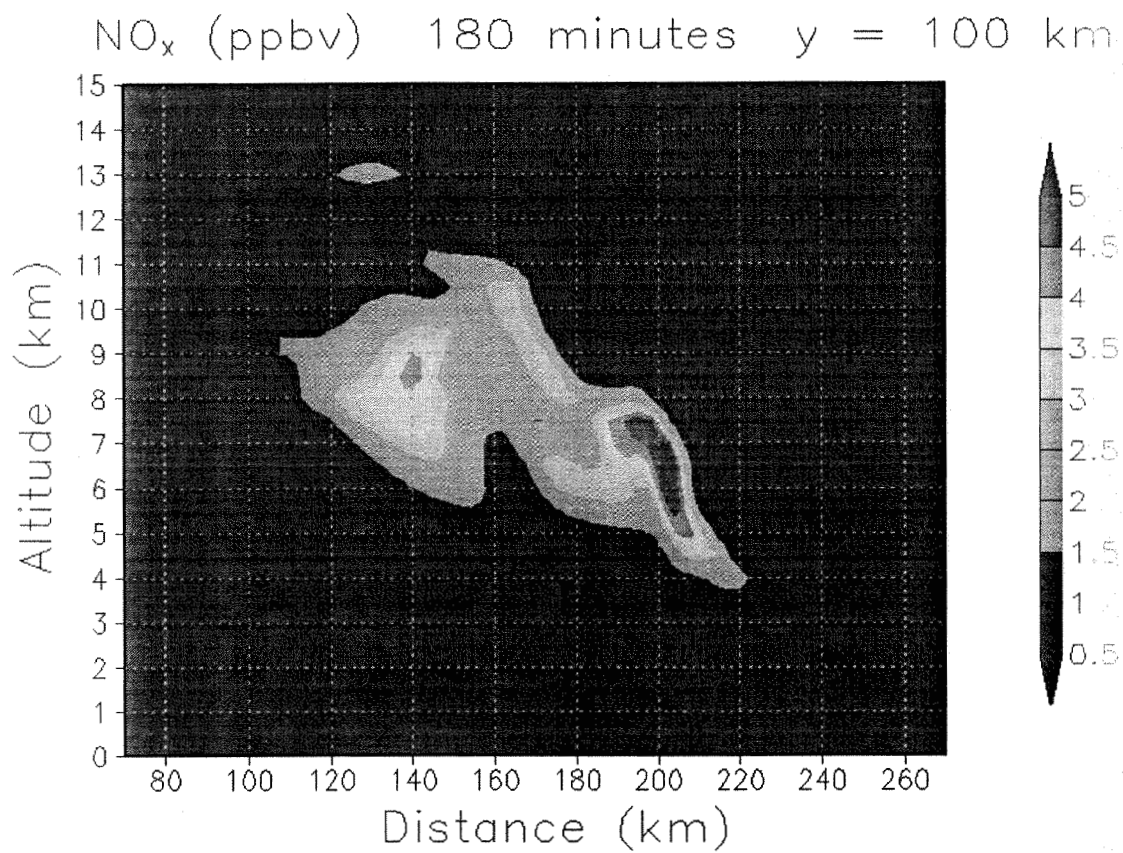954
955
956

## July 29 NLDN Flashes
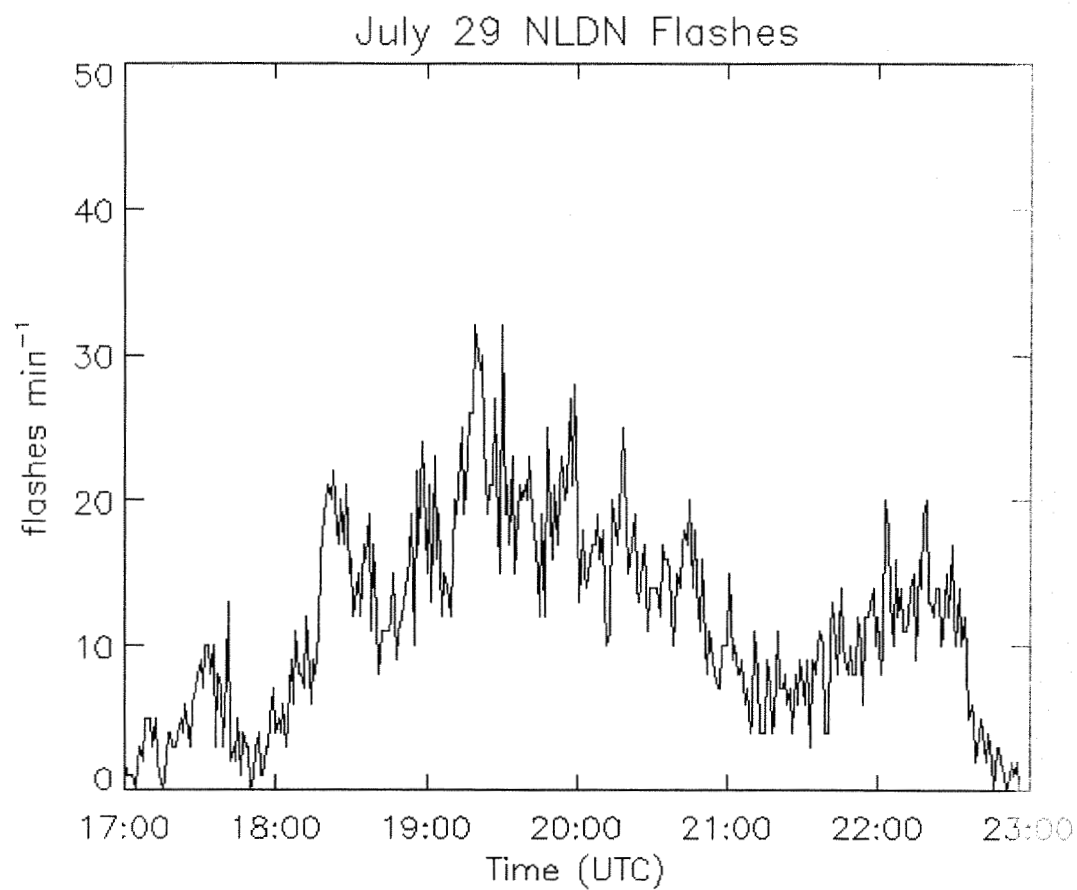
956
957
958     Figure 1. Time series of CG flash rates detected by the NLDN from 1700 to 2300 UTC
959     (1300 and 1900 LT) for the July 29 CRYSTAL-FACE storm.
960
961
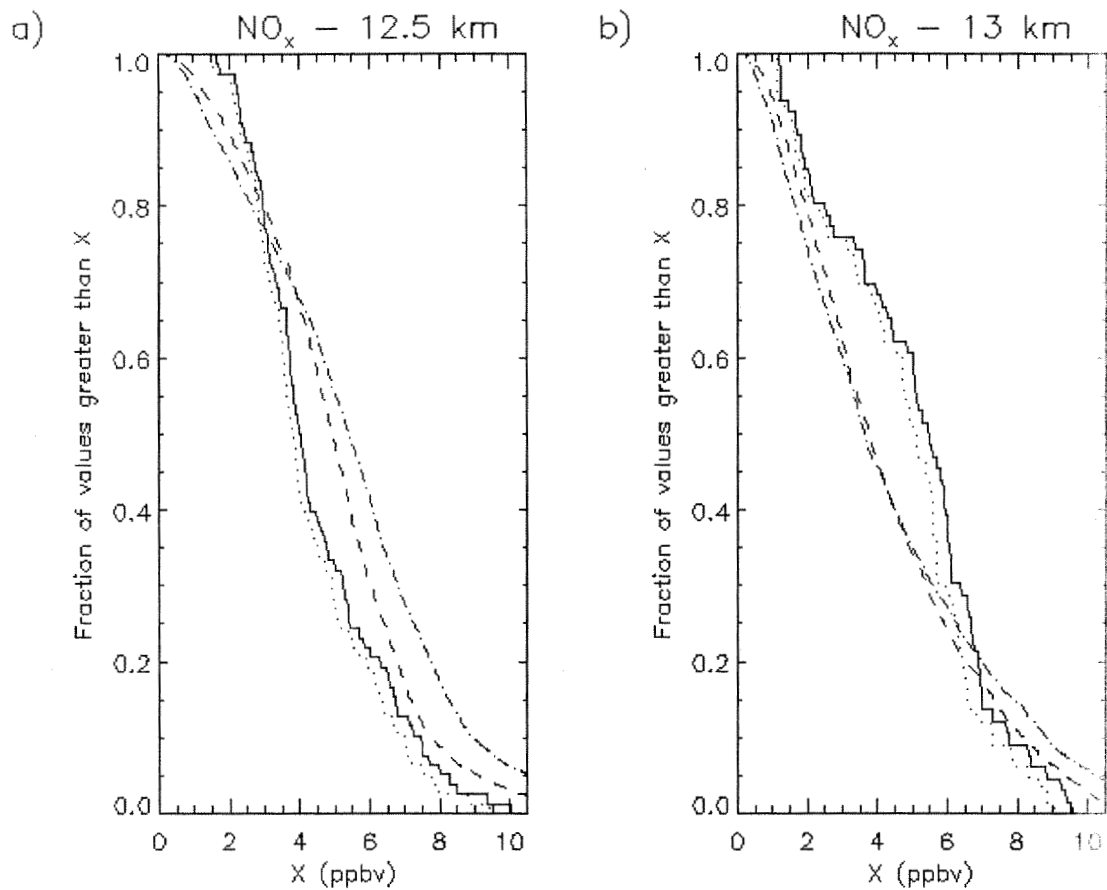
Figure 2. Pdfs of simulated and observed $NO_x$ at 12.5 km (a) and 13 km (b) for the July 29 CRYSTAL-FACE storm. Solid (dashed) line shows observed values assuming clear sky (cloud enhanced) photolysis rates. Dashed (dot-dashed) line shows simulated values assuming $P_{IC}/P_{CG}$ of 0.5 (0.6).

984
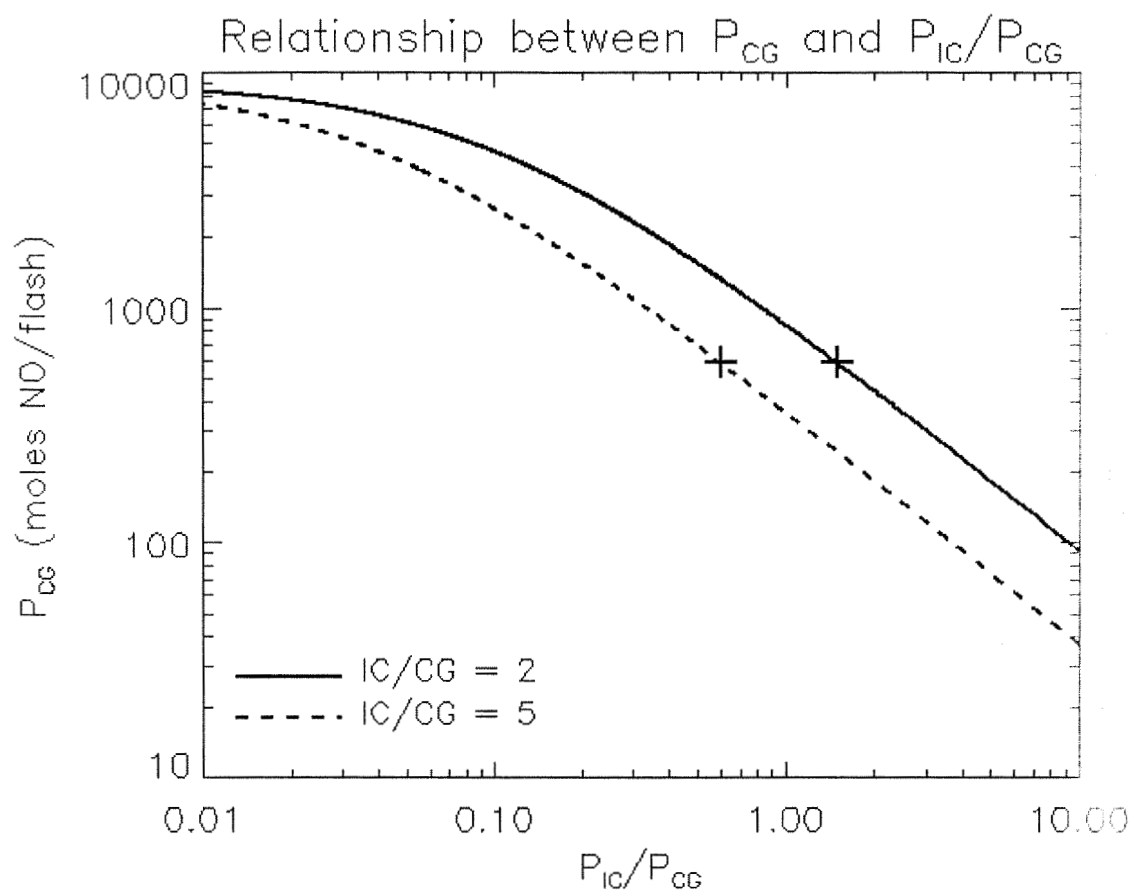


Figure 3. Relationship between $P_{CG}$ and the $P_{IC}/P_{CG}$ ratio necessary to match the column
mass of N computed from aircraft observations. Solid (dashed) line shows the
relationship when an IC/CG ratio of 2 (5) is assumed. Plus signs indicate the production
scenarios when $P_{CG}$ is assumed to be 590 moles NO per flash based on observed mean
peak current.
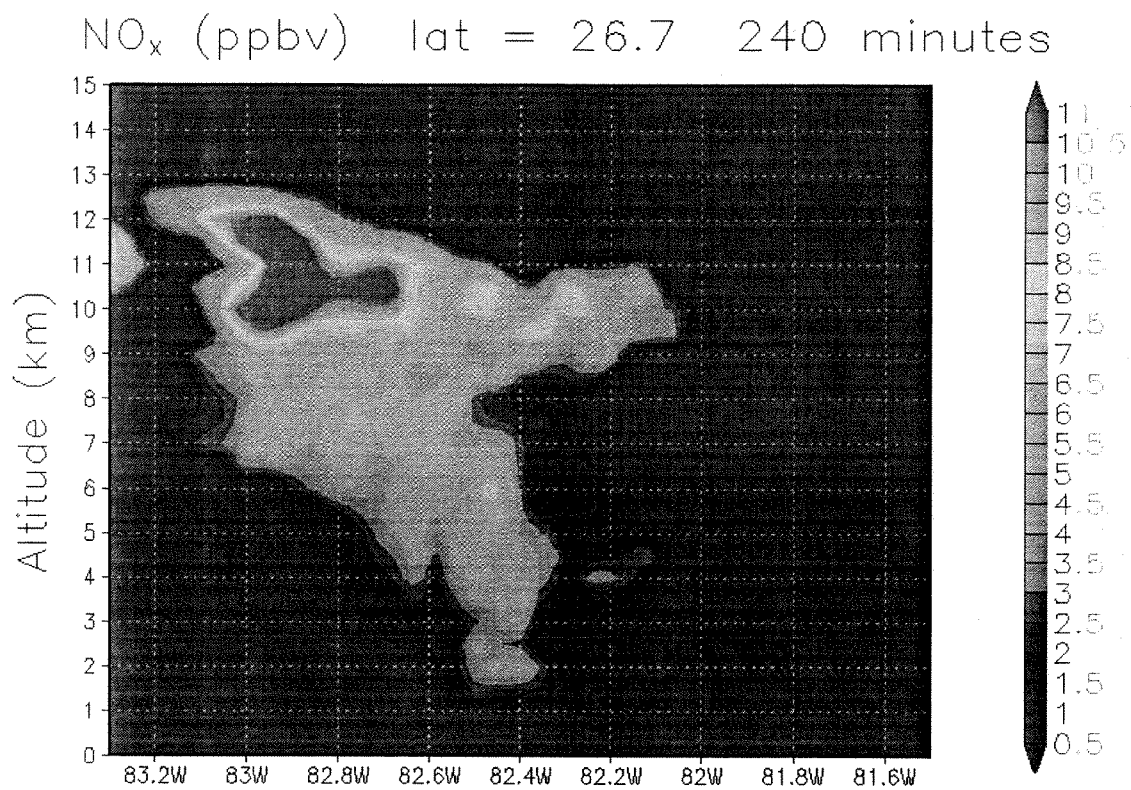
NOx (ppbv)   lat = 26.7   240 minutes

Figure 4.  Vertical cross-section of simulated $NO_x$ in the July 29 CRYSTAL-FACE storm (assuming $P_{CG}$ = 590 moles NO, $P_{IC}$ = 354 moles NO, and an IC/CG ratio of 5) at 240 minutes.
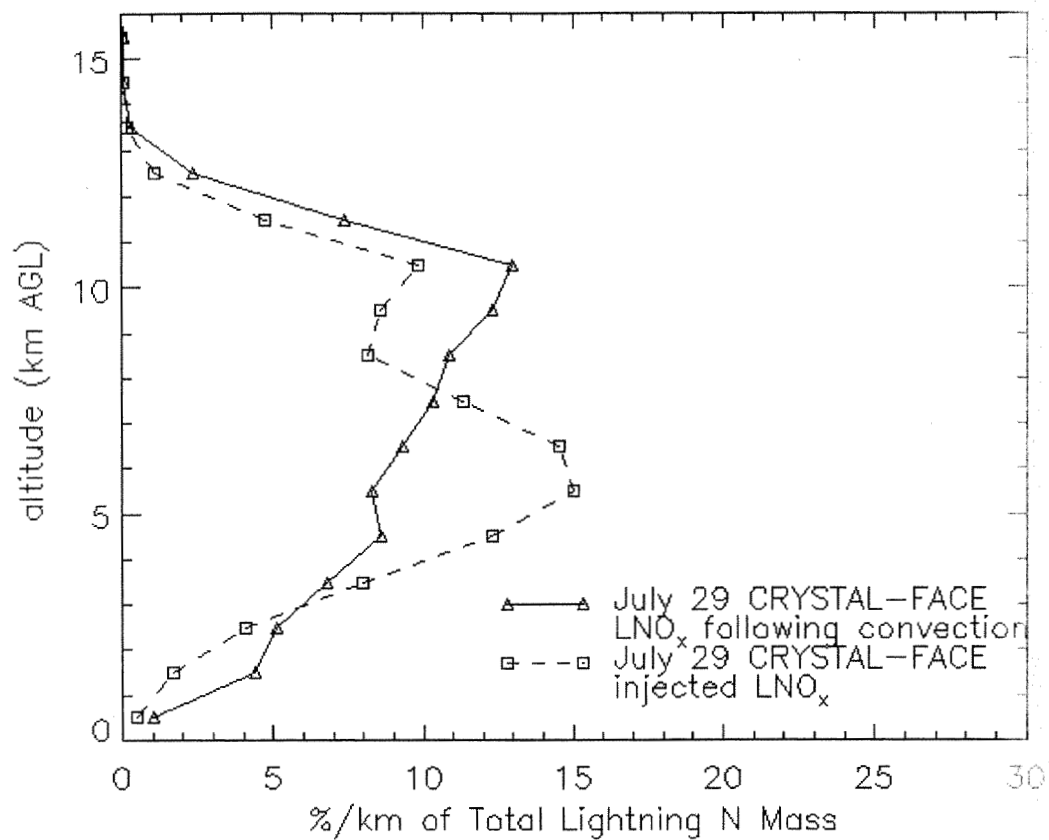
Figure 5. Vertical distributions of the percentage of $LNO_x$ mass per kilometer injected into the cloud and following convection for the July 29 CRYSTAL-FACE storm (assuming $P_{CG}$ = 590 moles NO, $P_{IC}$ = 354 moles NO, and an IC/CG ratio of 5).

## July 16 NLDN Flashes



1003
1004
1005    Figure 6. Time series of CG flash rates detected by the NLDN from 1900 to 2300 UTC
1006    (1500 to 1900 LT) for the July 16 CRYSTAL-FACE storm.
1007
1008
1009

NO$_x$ (ppbv)   180 minutes   y = 100 km

NO$_x$ (ppbv)   180 minutes   y = 100 km

1009
1010
1011    Figure 7.  Vertical cross-section of simulated NO$_x$ through the core of the July 16
1012    CRYSTAL-FACE storm assuming $P_{CG}$ = 700 moles NO and $P_{IC}$ = 630 moles NO at 180
1013    minutes.
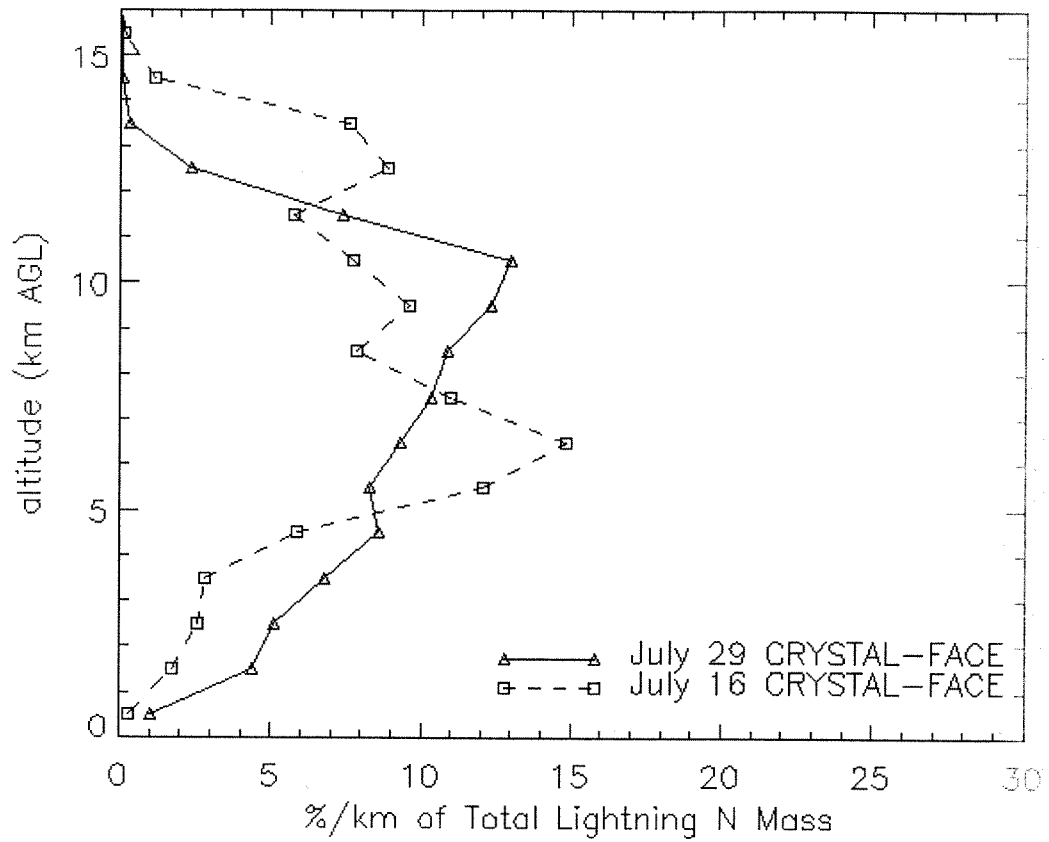
Figure 8. Vertical distributions of percentage of $LNO_x$ mass per kilometer following convection for two simulated subtropical storms.

1019
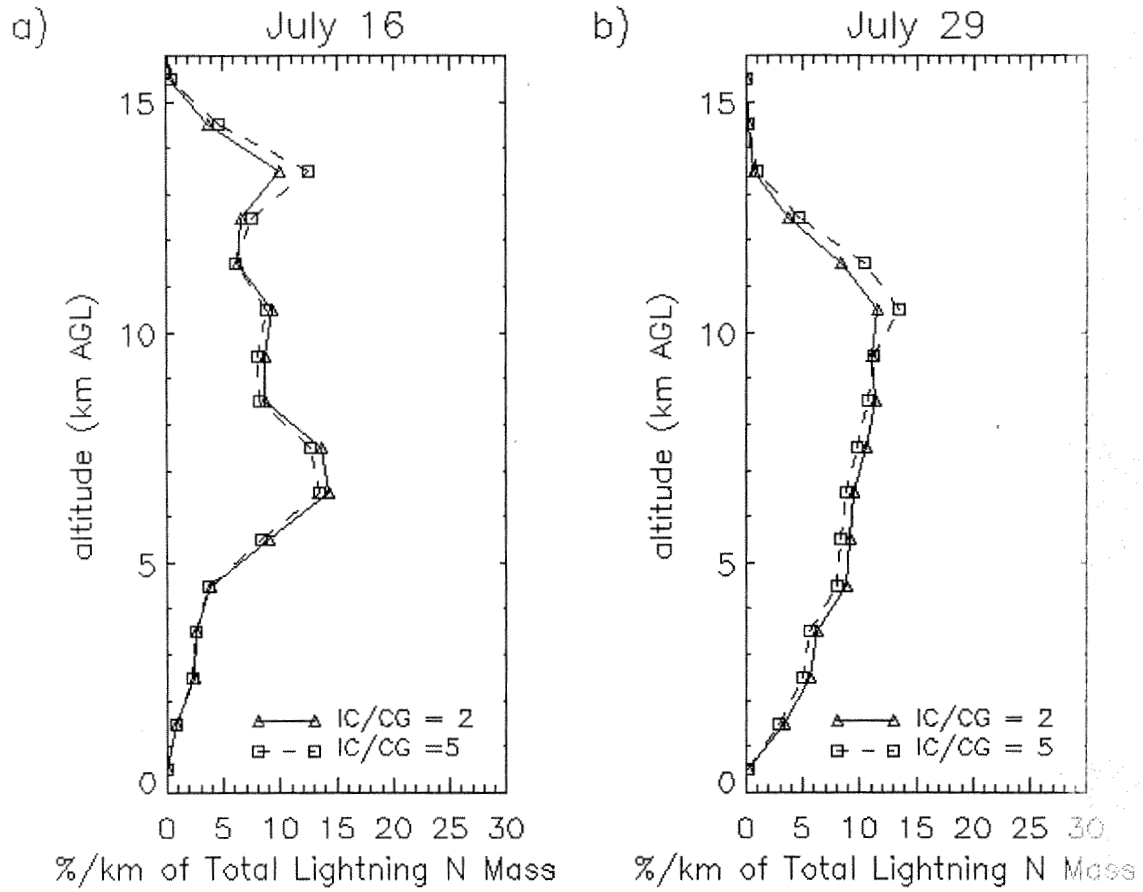


Figure 9. Vertical distributions of the percentage of $LNO_x$ mass per kilometer following convection for (a) the July 16 and (b) the July 29 CRYSTAL-FACE simulations assuming IC to CG ratios of 2 and 5.

NO$_x$ (ppbv)   180 minutes   y = 68 km
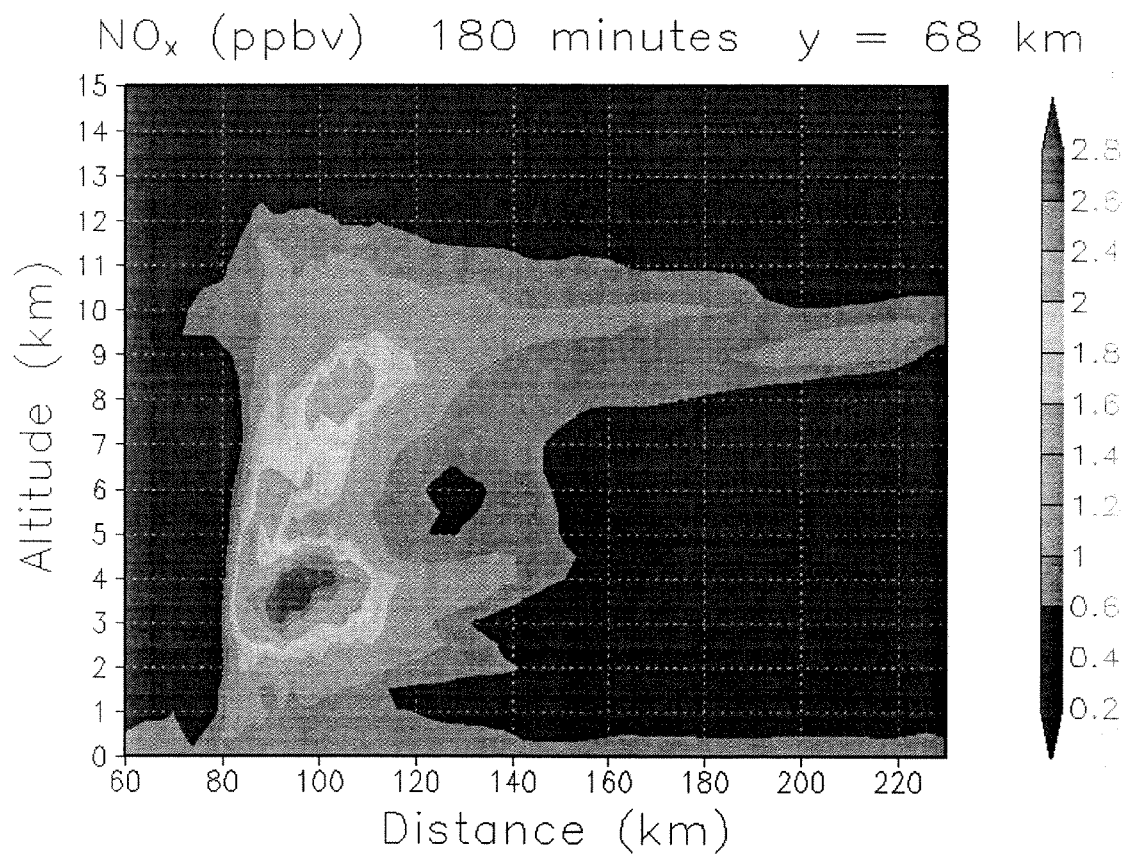
Figure 10. Vertical cross-section of simulated NO$_x$ through the core of the southern cell of the July 10 STERAO storm assuming P$_{CG}$=390 moles NO and P$_{IC}$=234 moles NO at 180 minutes.
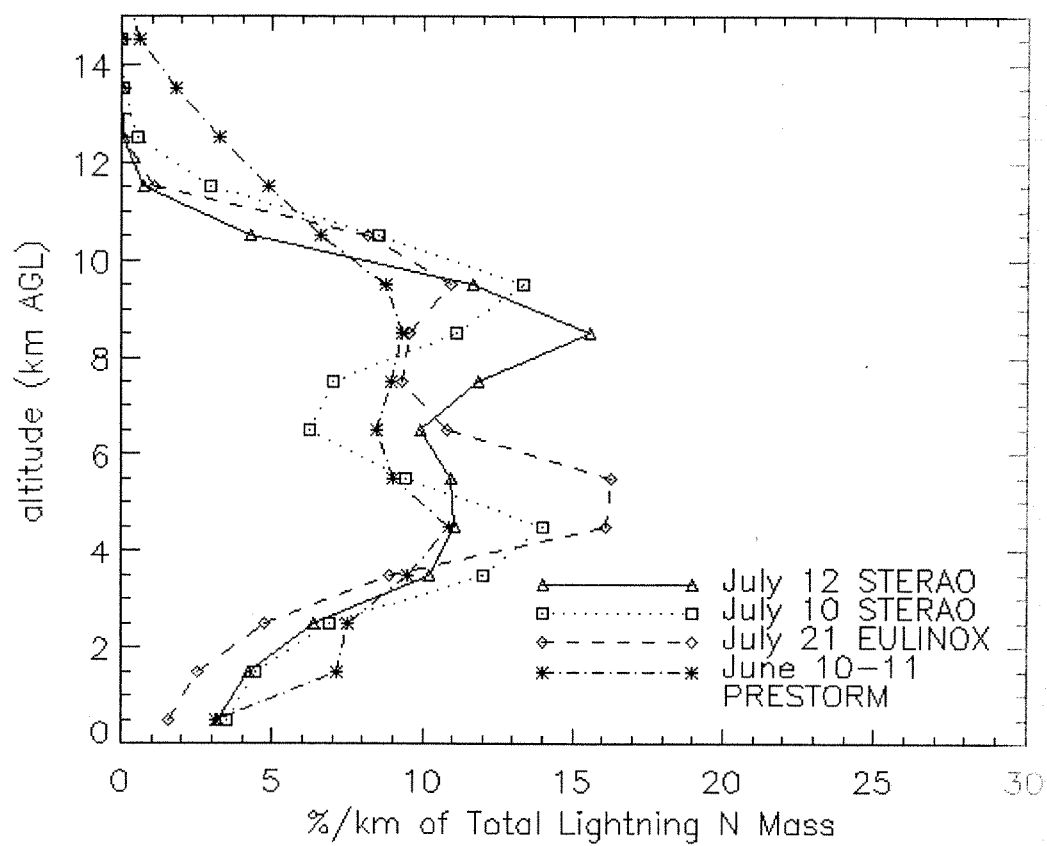
Figure 11. Vertical distributions of percentage of $LNO_x$ mass per kilometer following convection for four simulated midlatitude continental storms.
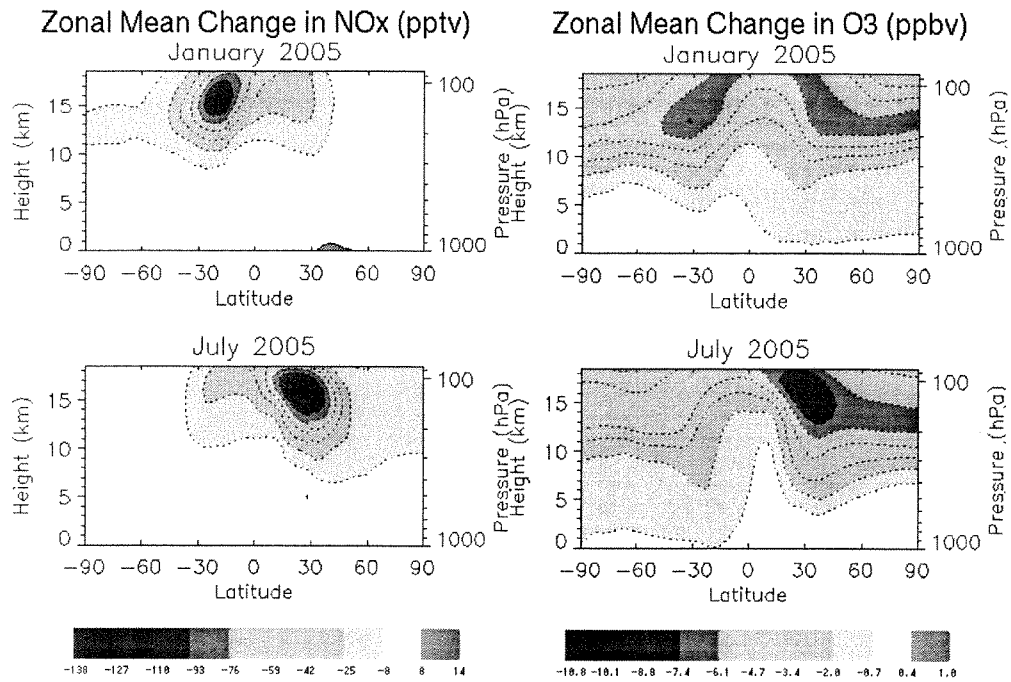
1032
1033
1034
1035
1036
1037
1038
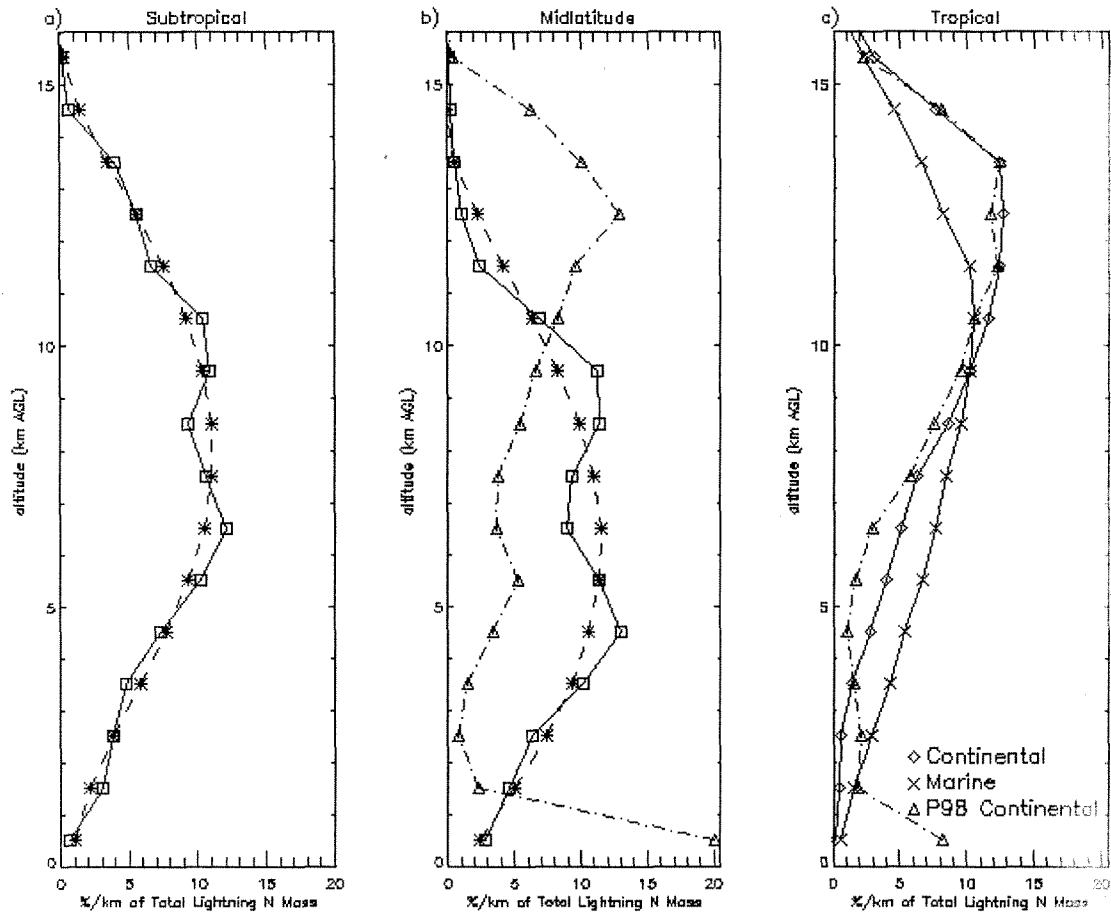
Figure 12. Average vertical distribution of percentage of $LNO_x$ mass per kilometer
following convection (solid) for the (a) subtropical and (b) midlatitude continental
regimes. Dashed line shows polynomial fit. Midlatitude continental profile from
Pickering et al. [1998] (dash-dot) is also shown in (b). Hypothetical tropical marine
profile (c) is based on extrapolating the subtropical average profile to a higher tropopause
regime while the tropical continental profile was constructed using the Pickering et al.
[1998] profile with the boundary layer maximum removed and that mass redistributed
into layers from 4 to 11 km.

1049
1050
1051
1052

## Zonal Mean Change in NOx (pptv)

### January 2005

### July 2005

## Zonal Mean Change in O3 (ppbv)

### January 2005

### July 2005

1053 Figure 13. Zonal mean change in NO$_x$ (pptv) and O$_3$ (ppbv) in January and July resulting
1054 from using the lightning NO$_x$ profiles in Figure 11 instead of the profiles from Pickering
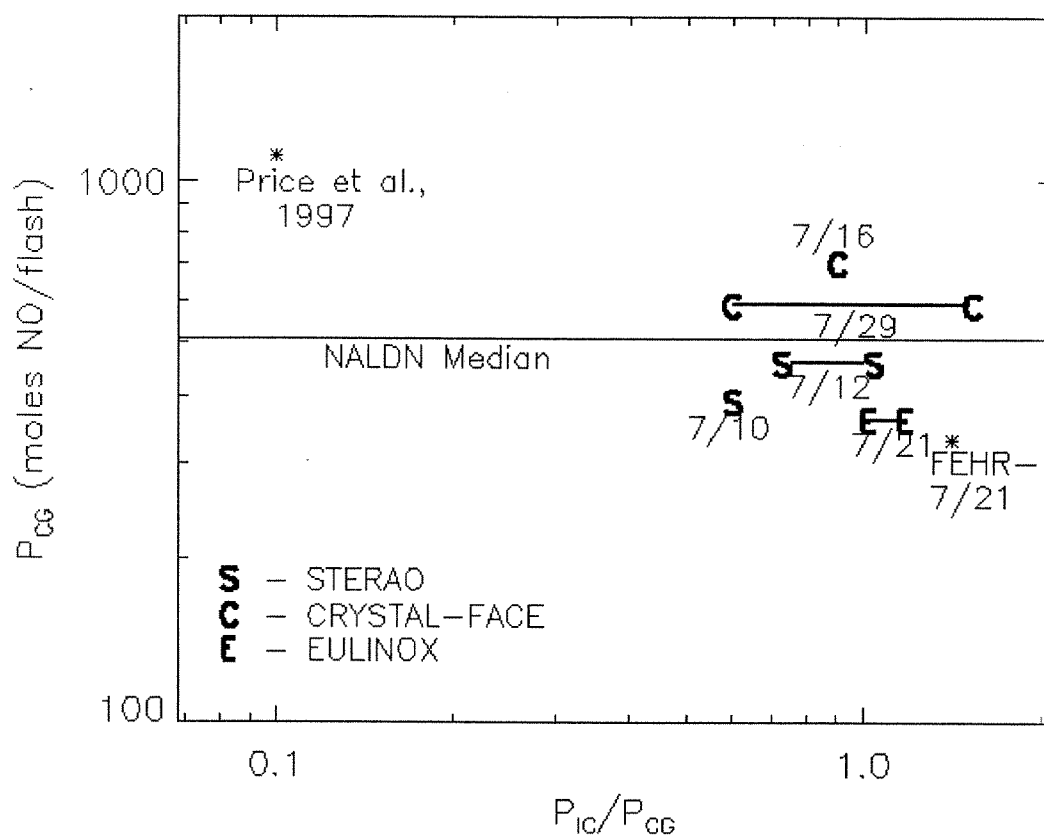1055 et al. [1998].

Figure 14. Estimated lightning $NO_x$ production scenarios for the July 16 CRYSTAL-FACE (C, 7/16), July 29 CRYSTAL-FACE (C, 7/29), July 10 STERAO (S, 7/10), July 12 STERAO (S, 7/12), and July 21 EULINOX (E, 7/21) storms. The bars in the 7/29 CRYSTAL-FACE, 7/12 STERAO, and 7/21 EULINOX storms indicate the estimate uncertainty. The Price et al., [1997] and Fehr et al. [2004] production scenarios are indicated by asterisks, as is the estimated value of $P_{CG}$ calculated assuming the NALDN median peak current from Orville et al. [2002].
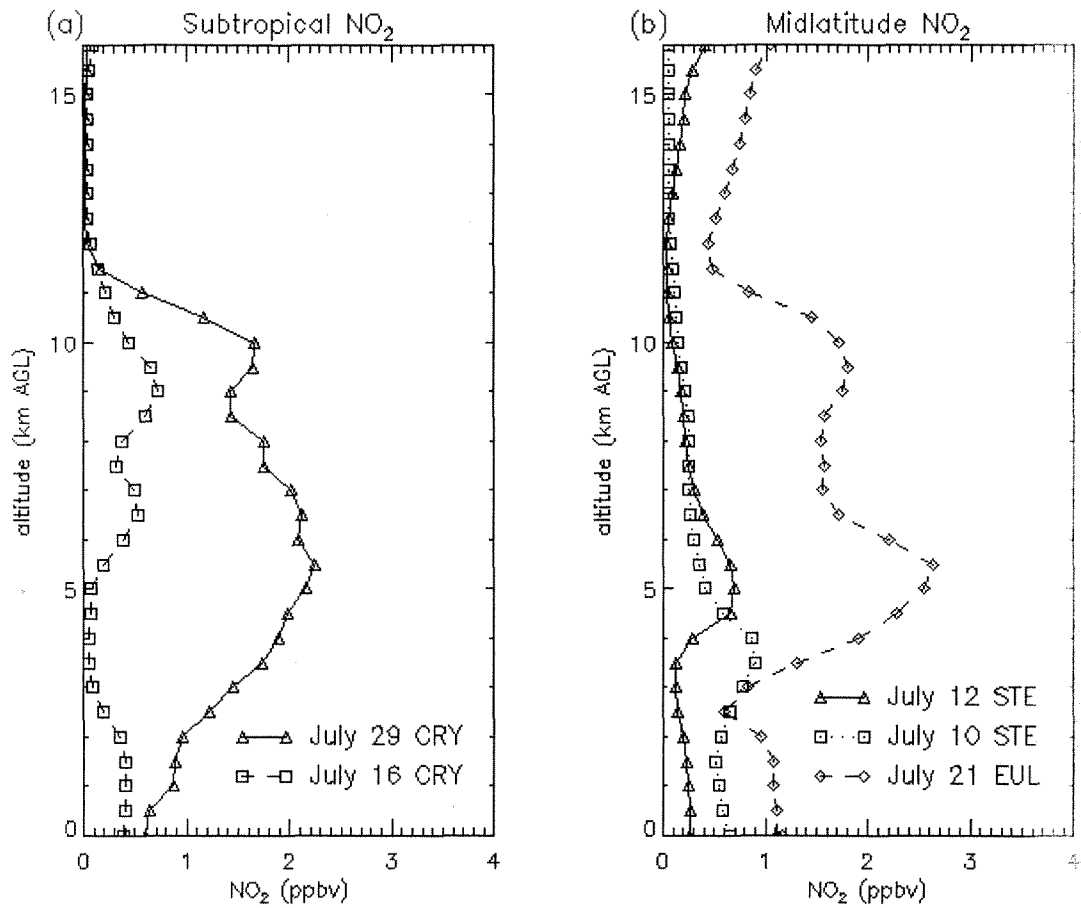
Figure 15. Average vertical profiles of $NO_2$ mixing ratio in the convective core region following simulated subtropical storms (a) and midlatitude storms (b).
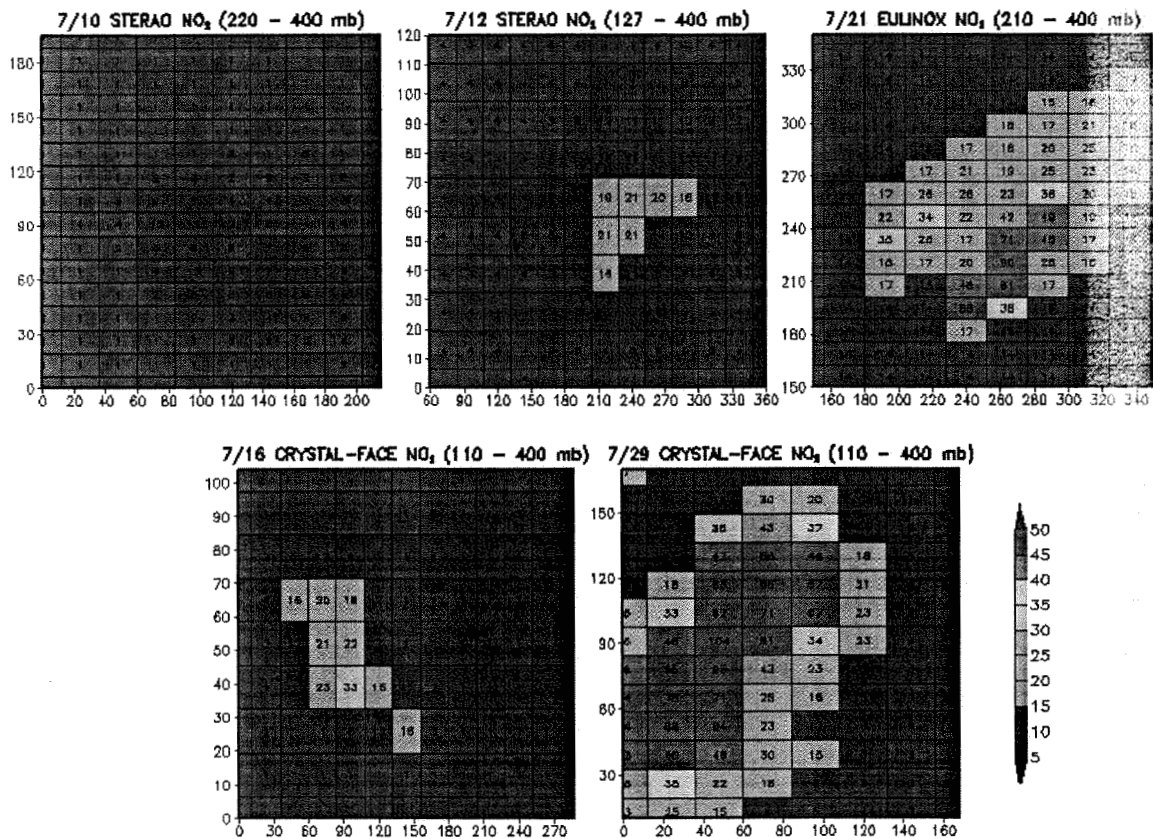
1072
1073    Figure 16.   Partial $NO_2$ columns ($10^{14}$ molecules $cm^{-2}$) from the tropopause to 400 hPa
1074    for CRYSTAL-FACE, STERAO, and EULINOX simulated thunderstorms.
1075